

**Palacký University Olomouc, Faculty of Science,  
Department of Geoinformatics**

**Paris Lodron University Salzburg, Faculty of Natural Sciences,  
Department of Geoinformatics**

# **GIS-BASED SOLAR PHOTOVOLTAIC POTENTIAL MODELLING IN THE URBAN AREA**

**Diploma thesis**

Author

**Rochamukti RIZCANOFANA**

Supervisor (Palacký University Olomouc)  
RNDr. Jan BRUS, Ph.D.

Co-supervisor (Paris Lodron University Salzburg)  
Univ.-Prof. Dr. Josef STROBL

**Erasmus Mundus Joint Master Degree Programme  
Copernicus Master in Digital Earth  
Specialization Track Geovisualization & Geocommunication  
Olomouc, Czech Republic, 2021**



Palacký University  
Olomouc



With the support of the  
Erasmus+ Programme  
of the European Union

## **ANNOTATION**

This thesis focuses on using a GIS-based approach to model solar PV potential in the urban area. The first stage of the thesis elaborates the literature review on the related topic to identify the most efficient GIS-based algorithm for calculating solar radiation, as it is one of the essential components in estimating the solar PV potential. Based on the literature review, the *r.sun* module was selected as the model algorithm. Morumbi district in São Paulo, Brazil, was chosen as the study area due to its data abundance, which can be accessed via the open data portal of São Paulo city (Geosampa). Furthermore, it deals with LiDAR point cloud data as the topographical data input, as well as atmospheric parameters and the modelling process to obtain solar radiation values in the study area. The later stage highlights the visualization workflow in designing a back-end and front-end environment of a web-map application containing the information of the rooftop solar PV potential in the study area. Additionally, a simple CityGML document is generated to store the information obtained by the modelling process in 3D. The result includes the amount of solar energy yield within a year as well as additional attributes such as the PV capacity, installation cost and CO<sub>2</sub> emission savings, which then visualized within an integrated spatial data infrastructure. In summary, the entire modelling workflow can be applied to solve a similar task in other study areas. It is expected that the result of this thesis could become guidance for the government, citizens, energy planners and solar energy engineers to evaluate the potential of solar energy within an urban area.

## **KEYWORDS**

Solar photovoltaic, solar radiation, LiDAR, GIS, urban, sustainability

Number of pages: 60

Number of appendixes: 5

This thesis has been composed by *Rochamukti Rizcanofana* for the Erasmus Mundus Joint Master's Degree Program in Copernicus Master in Digital Earth for the academic year 2019/2020 at the Department of Geoinformatics, Faculty of Natural Sciences, Paris Lodron University Salzburg, and Department of Geoinformatics, Faculty of Science, Palacký University Olomouc.

Hereby, I declare that this piece of work is entirely my own, the references cited have been acknowledged and the thesis has not been previously submitted to the fulfilment of the higher degree.

20. 05. 2021, Olomouc

Rochamukti Rizcanofana

## **ACKNOWLEDGEMENT**

*I would like to express my sincere gratitude to everyone who supported me during the process of writing this Master's Thesis. Without whom, I would not have been able to complete this thesis.*

*First and foremost, I would like to express the most profound appreciation to my advisors, RNDr. Jan Brus, Ph.D. from the Palacky University Olomouc and Univ.-Prof. Dr. Josef Strobl from the Paris Lodron University Salzburg, for their invaluable advice and insightful feedback throughout this thesis work. I would also like to thank Mag. Dr. Manfred Mittlböck from the Paris Lodron University Salzburg for his supportive assistance in solving the issue I encountered during the establishment of the spatial data infrastructure.*

*Furthermore, I would like to express my gratitude to the European Education and Culture Executive Agency (EACEA) and the European Union for granting me with the Erasmus Mundus Joint Master Degree (EMJMD) scholarship under the Copernicus Master in Digital Earth (CDE) programme, that provided funds towards the completion of the programme.*

*Also, I would also like to acknowledge all staffs at the Palacky University Olomouc and the University of Salzburg for their support throughout my study. In addition, I would like to thank my colleagues in the CDE programme, it has been great to know all of you during my study in Salzburg and Olomouc.*

*Finally, I am forever grateful for my family and friends, who always believe in me. I genuinely appreciate their unconditional support and encouragement.*

## ASSIGNMENT OF DIPLOMA THESIS

(project, art work, art performance)

Name and surname: Rochamukti RIZCANOFANA  
Personal number: R200661  
Study programme: N0532A330010 Geoinformatics and Cartography  
Field of study: Geoinformatics and Cartography  
Work topic: GIS-BASED SOLAR PHOTOVOLTAIC POTENTIAL MODELLING IN THE URBAN AREA  
Assigning department: Department of Geoinformatics

### Theses guidelines

The aim of this thesis study is to use GIS method to model the solar PV potential, particularly in the urban area. In order to achieve the aim, the following objectives will be conducted; to identify the GIS methodology to model the solar PV potential, assess the potential of solar PV in the urban area, particularly for electricity generation and visualise the estimation of solar PV potential per building's rooftop within an integrated spatial data infrastructure. The study will be using available datasets from open data sources and tools based on the GIS principle. The result of this thesis is expected to support the urban area development in accessing sustainable and economical energy resource, as it is also stated as of the UN Sustainable Development Goals (UN SDGs) number 9, affordable and clean energy. The student will attach all the collected datasets and all the animations to the thesis in digital form. The student will create a website about the thesis following the rules available on the department's website and a poster about the diploma thesis in A2 format. The student will submit entire text (text, attachments, poster, outputs, input and output data) in digital form on a storage medium and the text of the thesis in two bound copies to the secretary of the department.

Extent of work report: max. 50 pages  
Extent of graphics content: as needed  
Form processing of diploma thesis: printed  
Language of elaboration: English

#### Recommended resources:

- Agugiaro, Giorgio & Nex, Francesco & Remondino, Fabio & de filippi, Riccardo & Droghetti, Shamar & Furlanello, Cesare. (2012). Solar radiation estimation on building roofs and web-based solar cadaster. ISPRS Annals of Photogrammetry, Remote Sensing and Spatial Information Sciences. I-2. 10.5194/isprsannals-I-2-177-2012.
- Brito, Miguel & Redweik, Paula & Catita, Cristina & Freitas, Sara & Santos, Miguel. (2019). 3D Solar Potential in the Urban Environment: A Case Study in Lisbon. Energies. 12. 3457. 10.3390/en12183457.
- Dominguez, Javier & Martín Avila, Ana María & Amador Guerra, Julio. (2015). Applying LIDAR datasets and GIS based model to evaluate solar potential over roofs: a review. AIMS Energy. 3. 326-343. 10.3934/energy.2015.3.326.
- Dubayah, R. and P.M. Rich. 1996. GIS-based solar radiation modeling. pp. 129-134 In: M.F. Goodchild, L.T. Steyaert, B.O. Parks. C. Johnston, D. Maidment, M. Crane, and S. Glendinning (eds). GIS and Environmental Modeling: Progress and Research Issues. GIS World Books. Fort Collins, CO.
- Falklev, E. 2017. Mapping of solar energy potential on Tromsøya using solar analyst in ArcGIS. Master Thesis Publication: UiT The Arctic University of Norway. <https://hdl.handle.net/10037/12083>
- Fu, P. and P.M. Rich. 1999. Design and implementation of the Solar Analyst: an ArcView extension for modeling solar radiation at landscape scales. Proceedings of the Nineteenth Annual ESRI User Conference

- Gergelova, Marcela & Kuzevicova, Zofia & slavomír, Labant & Kuzevic, Stefan & Bobíková, Diana & Mižák, Jozef. (2020). Roof's Potential and Suitability for PV Systems Based on LiDAR: A Case Study of Komárno, Slovakia. Sustainability. 12. 10.3390/su122310018.
- Khan, Jibran. (2013). Solar Radiations Modeling of Karachi in a GIS Environment. 10.13140/RG.2.1.2122.7364.
- Murshed, Syed Monjur & Simons, Alexander & Lindsay, Amy & Picard, Solène & Pin, Céline. (2018). Evaluation of Two Solar Radiation Algorithms on 3D City Models for Calculating Photovoltaic Potential. 10.5220/0006789702960303.
- Nguyen, Ha & Pearce, Joshua. (2010). Estimating Potential Photovoltaic Yield with r.sun and the Open Source Geographical Resources Analysis Support System. Solar Energy. 84. 831-843. 10.1016/j.solener.2010.02.009.
- Prieto, Iñaki & Izkara, José & Usobiaga, Elena. (2019). The Application of LiDAR Data for the Solar Potential Analysis Based on Urban 3D Model. Remote Sensing. 11. 2348. 10.3390/rs11202348.

Supervisors of diploma thesis: **RNDr. Jan Brus, Ph.D.**  
Department of Geoinformatics

Date of assignment of diploma thesis: **November 9, 2020**

Submission deadline of diploma thesis: **May 6, 2021**

UNIVERZITA PALACKÉHO V OLOMOUCI  
PŘÍRODOVĚDECKÁ FAKULTA  
KATEDRA GEOINFORMATIKY  
17. listopadu 50, 771 46 Olomouc

L.S.

---

doc. RNDr. Martin Kubala, Ph.D.  
Dean

---

prof. RNDr. Vít Voženílek, CSc.  
Head of Department



# CONTENT

<b>LIST OF ABBREVIATIONS .....</b>	<b>6</b>
<b>INTRODUCTION .....</b>	<b>7</b>
<b>1 OBJECTIVES.....</b>	<b>8</b>
<b>2 METHODOLOGY.....</b>	<b>9</b>
<b>3 STATE OF THE ART .....</b>	<b>14</b>
<b>4 MODELLING THE SOLAR PV POTENTIAL .....</b>	<b>20</b>
4.1 LiDAR Point Cloud Data Processing .....	20
4.1.1 Merging Point Cloud Data .....	20
4.1.2 DSM Generation.....	20
4.2 Calculate the Annual Solar Radiation .....	21
4.2.1 Calculate Slope and Aspect.....	22
4.2.2 Annual Solar Radiation in Morumbi.....	22
4.3 Modelling Solar PV Potential .....	25
4.3.1 Building Suitability .....	25
4.3.2 Calculate Rooftop PV Potential Per Building .....	27
4.3.3 Additional Analyses.....	27
<b>5 VISUALIZATION .....</b>	<b>29</b>
5.1 Building a spatial database.....	29
5.2 Setup a server .....	32
5.3 Web-map application deployment .....	34
5.4 Store the building model in CityGML format.....	36
<b>6 RESULTS .....</b>	<b>37</b>
6.1 Analysis .....	37
6.2 Visualization of results.....	47
<b>7 DISCUSSION .....</b>	<b>55</b>
7.1 Data suitability .....	55
7.2 The modelling process.....	56
7.3 Visualization process .....	57
7.4 Future perspective .....	57
<b>8 CONCLUSION .....</b>	<b>59</b>
<b>REFERENCE AND INFORMATION SOURCES.....</b>	<b>60</b>
<b>REFERENCES AND INFORMATION SOURCES</b>	
<b>ATTACHMENTS</b>	

## LIST OF ABBREVIATIONS

Abbreviation	Meaning
BRL	Brazilian Real
CSS	Cascading Style Sheet
DEM	Digital Elevation Model
DSM	Digital Surface Model
DTM	Digital Terrain Model
ECMWF	European Centre for Medium-Range Weather Forecasts
GDAL	Geospatial Data Abstraction Library
GIS	Geographic Information System
GML	Geography Markup Language
HTML	HyperText Markup Language
IAG	Institute of Astronomy, Geophysics and Atmospheric Sciences
IDW	Inverse Distance Weighing
IMU	Inertial Measurement Unit
IRENA	International Renewable Energy Agency
JSON	JavaScript Object Notation
LoD	Level of Detail
kWp	kilowatt-peak
LiDAR	Light Detection and Ranging
MAE	Mean Absolute Error
MAPE	Mean Absolute Percentage Error
NHBC	National House Building Council
NREL	National Renewable Energy Laboratory
OGC	Open Geospatial Consortium
PV	Photovoltaic
RMSE	Root Mean Square Error
PDAL	Point Data Abstraction Library
SDI	Spatial Data Infrastructure
SQL	Structured Query Language
TIFF	Tagged Image File Format
UTM	Universal Transverse Mercator
WFS	Web Feature Service
WMS	Web Map Service
WMTS	Web Map Tile Service
XML	EXtensible Markup Language



# INTRODUCTION

CO<sub>2</sub> emission is one of the main factors that contribute to global warming. Electricity generation and industry are the two dominant CO<sub>2</sub>-emitting businesses, accounting for about 65 per cent of all energy-related CO<sub>2</sub> emissions in 2017 (IRENA, 2017). This phenomenon urges world leaders to commit to reducing CO<sub>2</sub> emission in every practice as it is ratified within COP21 Paris Agreement, including electricity generation. The contribution to climate change and global warming by the use of fossil energy in the electricity generation process becomes the ultimate reason for the transition to renewable energy resources such as hydropower, solar, wind, etc.

Following that, solar energy is one of the renewable energy resources that are easily accessible in terms of its abundance and maturity. The trend of solar photovoltaic installation cost also shows a downtrend from the past few years. Solar photovoltaic (PV) shows the sharpest decrease in costs in 2010-2019 at 82%, followed by a 47% concentration of solar energy (IRENA, 2020). Moreover, it also presents an advantage as it can be utilized in large-scale or small-scale. The latter refers to the utilization of the solar energy system or solar photovoltaic on a building. The energy supply generated by the widespread installation of photovoltaic systems in urban areas will provide a long-term contribution to energy demands (Amado & Poggi, 2014).

One of the steps required to be carried out during the early-stage development of a solar PV system is calculating the amount of solar radiation, which is an essential parameter for identifying solar energy potential. In-situ measurement using a pyranometer instrument might be the most accurate solution to obtain the solar radiation value. However, it can only cover a limited area. Therefore, if the calculation of solar radiation is required for larger-scale areas, for instance, a village, district, or city, the in-situ measurement can be tedious and time-consuming.

Solar radiation is also influenced by the topographical condition as well as meteorological and atmospherical characteristics of each location. GIS, which involves location intelligence and spatial analysis, could become a solutive approach to calculate solar radiation properly. The geoinformatics technology application is quite broad. Nevertheless, it can be orchestrated to provide high-resolution topographical data input and calculate solar radiation in an urban area using GIS analysis. Further analysis based on GIS can be conducted to obtain other attributes related to solar energy such as power, PV capacity, CO<sub>2</sub> emission savings, and many more.

This thesis highlights the prospect of GIS technology to be used for modelling the potential of solar energy in the urban area. High-resolution LiDAR point cloud data and atmospherical parameters from various open data portal are used in this research. The research area, in this case, is Morumbi district in São Paulo is chosen based on the building density characteristic and data availability. The result includes the amount of solar energy within a year, and other related components will then be visualized in an integrated spatial data infrastructure.

# 1 OBJECTIVES

This thesis is aimed at using the GIS approach to model the potential of solar rooftop PV in the urban area, which will support the initial process in designing a proper solar photovoltaic system.

In order to achieve the aim previously stated, the work in this thesis will be carried out according to the following objectives:

1. Identify Geographic Information System (GIS) based algorithm to model the solar PV potential.
2. Assess the potential of solar PV for electricity generation in the urban area.
3. Visualize the estimation of solar PV potential on the rooftop per building within an integrated spatial data infrastructure.

It is expected that the result of this thesis could become guidance for solar energy engineers to evaluate the potential of solar energy within an urban area. As the hassle that usually occurs in the early stage solar PV deployment by the uncertainty of the solar energy potential can be eliminated. In addition, providing a visualization of the solar energy potential can raise awareness among the institution and residents about the solar energy potential in their area, which will succeed the green energy transition and sustainable urban development accordingly.

## 2 METHODOLOGY

### Study Area

The study area is located in the city of São Paulo, Brazil. São Paulo lies in the southeast region of Brazil, about 350 km southwest of Rio de Janeiro and 50 km inland from the Atlantic Ocean (Schneider et al., 2020). The city covers a total area of 1,493 km<sup>2</sup> with 12.04 million inhabitants (São Paulo Turismo (SPTuris), 2017). São Paulo has a pleasantly mild climate. July is the coldest month, with an average temperature of 14°C and seasonal cold winds. The warmest month is February, with a mean temperature of 21°C. Rainfall is plentiful, particularly during the summer months of October to March, exceeding 1,422 mm each year (Schneider et al., 2020). Initially, the author intended to use the entire city of São Paulo for the study area. However, during the computation process, a large study area consumed too much of the PC memory and the computation time took a considerably long time. Hence, the research area is being reduced to a district scale. The Morumbi district is then selected as the focus of the research.

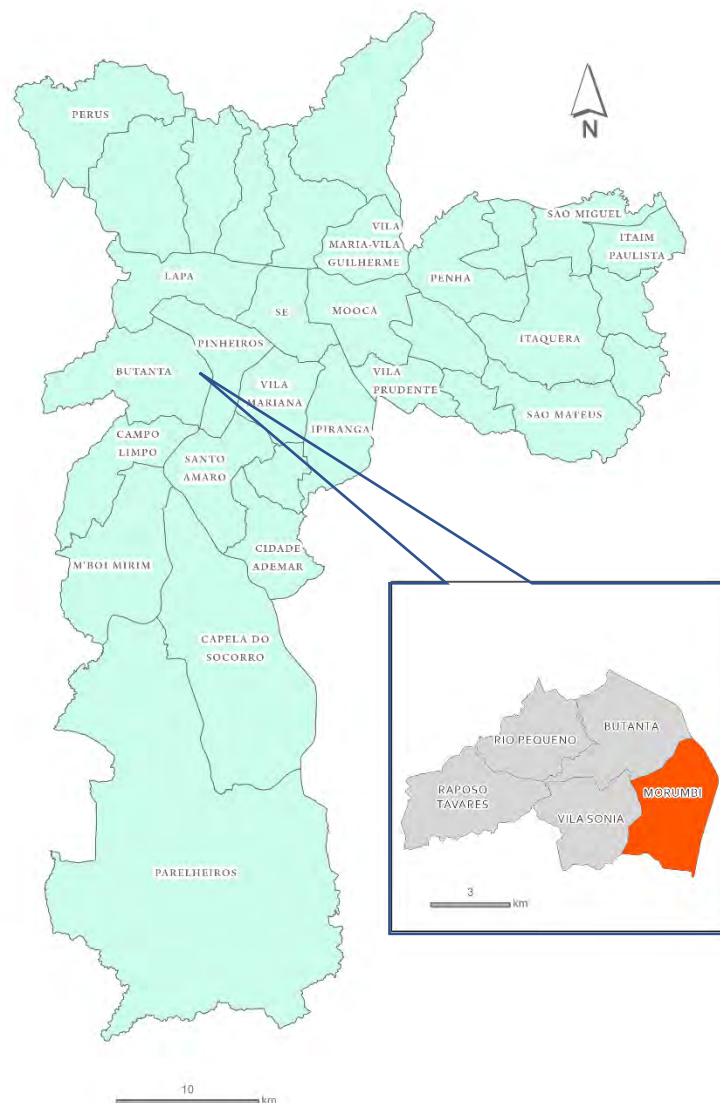


**Figure 1 Map of the research area. The vector boundary is provided by <http://geosampa.prefeitura.sp.gov.br/>. Created in ArcGIS Pro**

Morumbi district in the subprefecture Butanta, city of São Paulo, Brazil, is situated in the southwestern part of the city of São Paulo. The approximate coordinate of Morumbi district is 23°36'00"S and 46°43'6.00"W. It covers an area of 11.47 km<sup>2</sup>. According to the 2010 census, the total population has reached 46,957. The northern side of the district shares border with Butanta and Pinheiros district, Itaim Bibi district to the east, Santo Amaro district to the south, and Vila Sônia to the west. Morumbi is known as a residential district and famous as the area where wealthy people in São Paulo live. The total number of buildings in the area is 15,121, containing residential, commercial, industry, and government offices. One of the city landmarks is also located in the area, Morumbi stadium or *Estádio do Morumbi*. Residential buildings type in Morumbi varies, from high-rise condominium, landed house and *favela* (slum).

### **Data sources**

The data used in this thesis were entirely derived from multiple non-commercial sources and open data portals. It is intended to support the principle of data openness and transparency. The open data source is non-binding and fully free, also accessible via the internet. Therefore, the complicated procedure in data requests can be avoided. The detailed information about data specification, including the source of each data item, is the following:

#### **1. LiDAR point cloud**

Topographical data are required in calculating solar radiation to identify the solar geometry and the absorption level of the solar energy on each surface. The point cloud data used in this thesis were derived from the city of São Paulo data portal (Geosampa: <http://geosampa.prefeitura.sp.gov.br/>). The point density is 18 points/m<sup>2</sup> for all returns and five points/ m<sup>2</sup> for the first return. The height accuracy of the data is  $\pm 0.20$  m. The point cloud data are already classified into five categories, soil, building, vegetation, road works and other features. According to its metadata, the data obtained by LiDAR technology in 2017 with the sensor attached to a helicopter. The classification was performed by the Consortium Green-SP and validated by the city of São Paulo. Point cloud data are available for download in the .LAZ file format, which is the compressed version of the LAS point cloud data format. The projection system of the data is SIRGAS-2000 UTM 23S.

#### **2. Building footprint**

Building footprint data was also downloaded from the Geosampa portal. The data is available in a 1:1,000 scale Shapefile format. The projection system is SIRGAS-2000 UTM 23S. However, the building polygons contain *favela* were not included.

#### **3. District boundary**

For data masking purpose during the analysis, district boundary data were also downloaded from the Geosampa portal. It is available in Shapefile format.

#### **4. Linke turbidity**

Linke turbidity (TL) or atmospheric absorption and scattering value were used for one of the input parameters in GRASS GIS for solar radiation calculation. The data were derived from the Solar radiation Data (SoDa) database, a solar energy-related data provider that originated from a European project led by Mines ParisTech. The data portal is currently managed by Research Center OIE and Transvalor S.A. from France. The data are available on a global scale, gridded raw TIFF format, and approximate cell size of 5'.

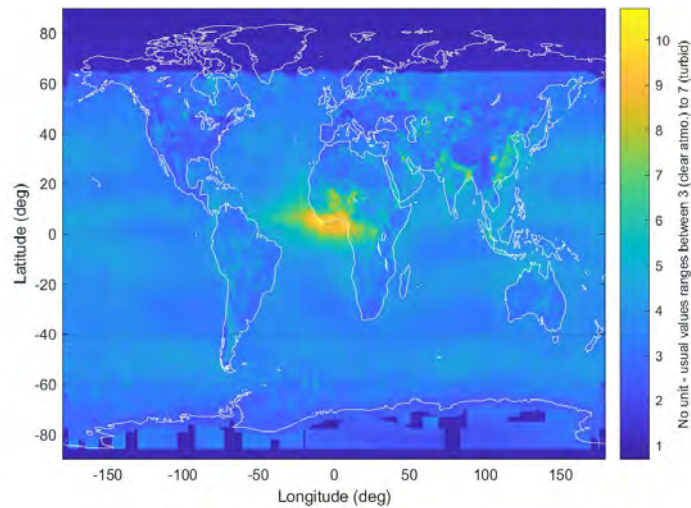


**Figure 2 Sample of Linke Turbidity data in January**  
(MINES ParisTech / Transvalor, 2021)

## 5. Surface Albedo

Surface albedo is unitless, and the value ranges from 0 to 1. Surface albedo values or solar flux per unit area were obtained from an in-situ measurement from the Institute of Astronomy, Geophysics and Atmospheric Sciences (IAG) in São Paulo that was published by Ferreira et al. in 2011. IAG conducted the measurement in 2004, hence, surface albedo data from the Copernicus Global Land service, which has a 1-km grid, were used for interpolation. In practice, the energy difference between dynamic albedo and constant albedo values as the input parameter is insignificant (Wang, 2015). However, since surface albedo values are available in the study area, the author decided to include dynamic surface albedo values for the model parameter.

## 6. Diurnal irradiation and solar radiation

Diurnal irradiation data were used to calculate clear-sky index values for obtaining solar radiation values in the actual sky condition. The solar irradiation of the city of São Paulo was obtained by submitting a request form to the IAG meteorological station (IAG-USP). Irradiation data is recorded from a bimetallic actinograph instrument which is installed on top of the IAG-USP building. Solar radiation data were collected from the Brazilian Laboratory of Modeling and Studies of Renewable Energy Resources (LABREN) for validation purpose.

## 7. Miscellaneous data

Miscellaneous data include solar photovoltaic (PV) specification and installation guide as well as solar energy market in Brazil. The data were derived from the United States Natural Renewable Energy Agency (NREL) and Americadosol project report.

## Software and Hardware

The hardware used in this research is a personal notebook with the specification below:

- System model: Dell XPS 13 9343
- Operating system: Windows 10 Home 64-bit (10.0 Build 19041)
- Processor: Intel® Core™ i5-5200U CPU @2.20GHz (4 CPUs), ~2.2GHz
- Memory: 8,192 MB

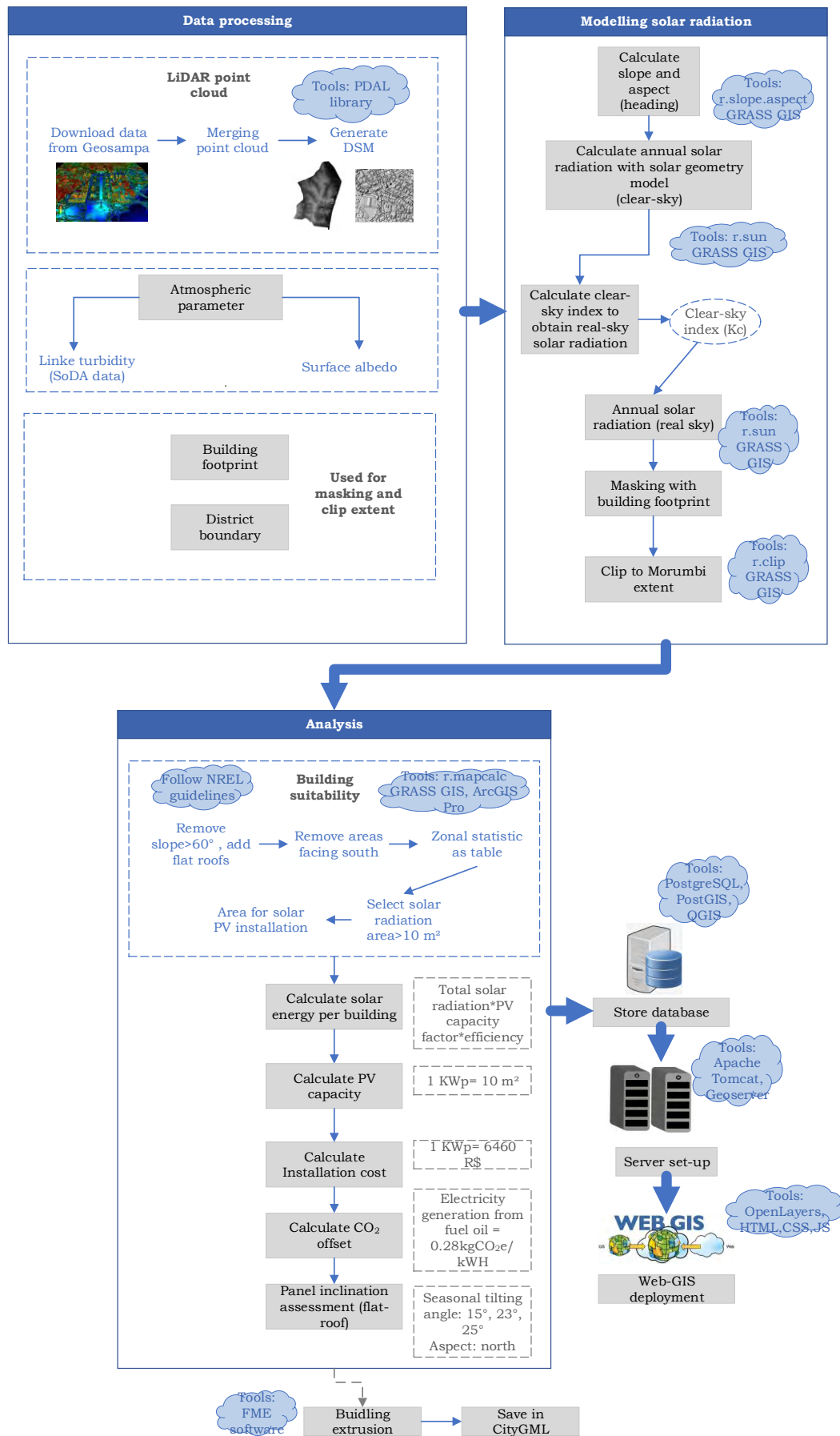
There were multiple software and programming languages that were utilized in this research. Initially, the processing step was intended to be carried out by only using open-source software. However, some geoprocessing tools from commercial software, for instance, Zonal Statistics as Table in ArcGIS Pro and CityGML extraction in FME, could not be run in open-source software, and the scripting option would take too much time to be deployed. Therefore, both commercial and open-source software were utilized in this thesis. The following table shows the software version and license type:

Table 1 Software and programming language

<b>Software/programming language</b>	<b>Version</b>	<b>License</b>	<b>Usage</b>
PDAL	2.2.0	Open	Point cloud data processing
GRASS GIS	7.8.2	Open	Solar radiation, raster calculation
Python	3.7	Open	Scripting
QGIS	3.12.2	Open	Feature editing
ArcGIS Pro	2.7.2	Commercial	Zonal statistic, feature attribution
FME (Safe Software)	2020.2	Commercial (free student license)	Data format conversion, building extrusion
PostgreSQL+ PostGIS	12	Open	Database management
Apache Tomcat	9.0.0	Open	Local server setup
Geoserver	2.18.2	Open	Spatial server
HTML	5	Open	Web map application
JavaScript	1.5	Open	Web map application
Openlayers	6.5.0	Open	Web map application
Microsoft Office	Professional Plus 2019	Commercial	Thesis writing and presentation

## Workflow

The work in this thesis was conducted within five main stages. The first stage was the data collection and processing, which included downloading LiDAR point cloud data, atmospheric parameters, building footprint and Morumbi district boundary. Afterwards, the workflow continued with modelling solar radiation, using data inputs and parameters that had been processed. The third stage was analyses to obtain additional attributes that will be included in the final visualization. The next stage was the visualization part that covered database management, server setup and web-GIS deployment. Lastly, storing building models and solar energy potential attributes into CityGML format. The entire workflow of the entire step carried out in this thesis is depicted in Figure 3.



**Figure 3 Workflow of the methodology**



### 3 STATE OF THE ART

#### Light Detection and Ranging (LiDAR)

LiDAR has proven itself a reliable tool for gathering dense and precise elevation data through landscapes, shallow-water environments, and project sites. This active remote sensing method is comparable to radar, but instead of radio waves, it uses laser light pulses (NOAA, 2012).

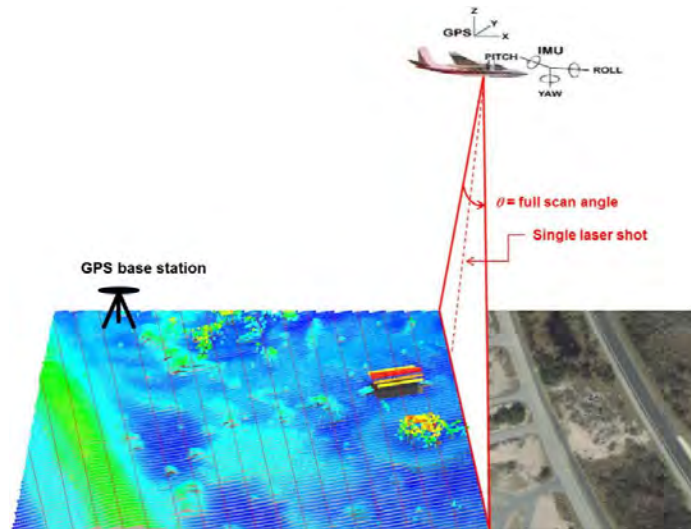


**Figure 4 Schematic diagram of airborne lidar performing line scanning (NOAA, 2012)**

A laser device, an inertial navigational measurement unit (IMU), which constantly records the aircraft's orientation, a high-precision airborne Global Positioning System (GPS) unit, which records the aircraft's three-dimensional position, and a computer interface that manages communications compose a LIDAR system which works from an airborne platform (USDA, 2008). The LiDAR theory is identical to Electronic Distance Measuring Instrument (EDMI), in where a laser (pulse or continuous wave) is launched from a transmitter, and the reflected energy is absorbed. The distance between the transmitter and reflector is calculated using the time of travel (ToT) of this laser (Lohani, 2010). The reflector could have been natural or artificial, such as a prism. In the case of ranging LiDAR, this distance is one of the key measurements that provide the reflector coordinates when combined with other measurements (Lohani, 2010). Post-processed LiDAR data is in the form of point clouds. Raw point clouds have the information of x,y, and z coordinates, as well as additional attributes, including GPS time stamps. After the raw data are being post-processed, each point represents the elevation of the surface on a specified coordinate (Esri, 2021).

#### Digital Elevation Model (DEM)

DEMs are gridded digital representations of terrain, with each pixel value indicating a height above a datum (Hawker et al., 2018). There are two forms of DEMs, a Digital Surface Model (DSM) and a Digital Terrain Model (DTM). A DSM is an elevation model that represents the Earth's surface and includes all objects (Contreras et al., 2020). In contrast, Digital Terrain Model (DTM) is a bare land surface model, which is supposedly free of trees, buildings or other non-ground objects (Zhou, 2017).

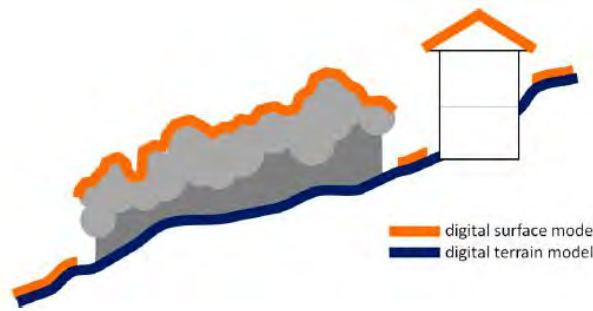


**Figure 5 Digital Surface Model vs Digital Terrain Model (Polidori & Hage, 2020)**

DSM and DTM can be generated from point cloud data, including LiDAR using interpolation methods. Lloyd & Atkinson (2002) published research about the comparison of IDW, Kriging and trends. The research concludes that the IDW is more suitable for generating the DSM in the urban area with high point density, whereas Kriging is more acceptable for point cloud data with low point density. According to Bafghi et al. (2016), the IDW performs better in filling holes during the DSM generation process. Therefore, in this thesis, DSM as the topographical data input was generated using the IDW method, which runs on Point Data Abstraction Library (PDAL).

### **Principle of Solar radiation**

Solar energy or solar radiation refers to the amount of energy produced by the sun. The amount of solar radiation intercepted by the Earth varies due to changes in the sun-earth distance day-to-day variations in the spectral spectrum caused by solar activity and atmospheric attenuation (Wald, 2018). There are three types of solar radiation spectrum that reach the Earth's surface, direct, diffuse and reflected solar radiation. The illustration of direct, diffuse and reflected solar radiation is depicted in Figure 6.

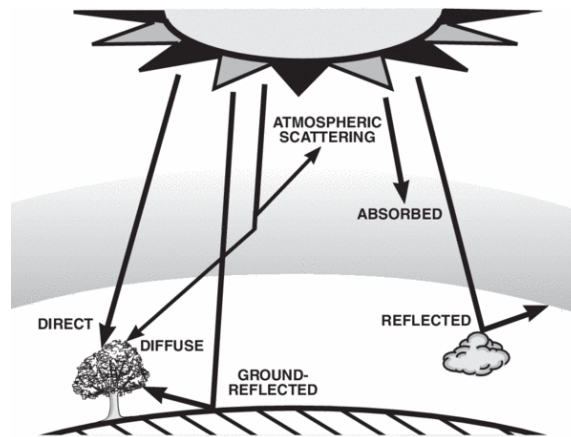


**Figure 6 Direct, diffuse and reflected solar radiation (Newport, 2021)**

Direct solar radiation is the solar energy that reaches the Earth's surface without being scattered in the atmosphere. Direct solar radiation drops as the elevation decrease, and as solar radiation passes through the atmosphere, the farther it travels to the lower surface elevation, the more influence from water vapour, aerosol, and mixed gas, hence the attenuation is more significant (Wang, 2019). The solar radiation influenced by this phenomenon is called diffuse solar radiation. The reflected radiation is the amount of solar radiation reflected from Earth's surface, which its proportion is relatively small and often is neglected in the solar radiation calculation (Esri, 2021). The sum of direct, diffuse and reflected component is global solar radiation or GHI which is used in most algorithms to calculate the total amount of solar radiation.

In some literature, solar energy is frequently expressed in two terminologies, irradiance and irradiation. The former is the instantaneous energy received by Earth's surface from the sun per unit time ( $\text{W}/\text{m}^2$ ) (Hofierka & Suri, 2002). The latter terminology is the amount of solar energy falling on an area in a given period ( $\text{Wh}/\text{m}^2$ ) (Hofierka & Suri, 2002).

### **Solar radiation calculation based on GIS**

There are available methods to determine the solar radiation value on a surface. Solar radiation can be measured by a pyranometer to identify global solar radiation or by a pyrliometer for measuring direct beam solar radiation. In addition to atmospheric attenuation, sun azimuth and altitude, the slope and aspect of the surface, and the relative orientation of the neighbouring surfaces affect the amount of solar radiation (Mamassis et al., 2012). Thus, GIS that works with spatial and geographic data could be a potential approach in predicting solar radiation.

One of the GIS-based algorithms for calculating solar radiation is *Solar Flux* by Dubayah & Rich (1995). The algorithm was implemented in ARC/INFO and GRID GIS platform. It takes a topographic surface as the input, as well as latitude, measurement time period, and transmittivity, and outputs of direct radiation flux, length of direct radiation, sky view factor, hemispherical estimates of horizon angles, and diffuse radiation flux for each location (Dubayah & Rich, 1995). The limitation in using this algorithm is that this algorithm was implemented in ARC/INFO, which its manufacturer, Esri, no longer supports.

The *Solar analyst* model developed by Esri is using the principle of the hemispherical viewshed. The algorithm works by calculating an upward-looking hemispherical viewshed according to the topography, then overlay it on a direct sun map and diffuse sky map, and iterating the process on every surface location to generate the insolation map (Esri, 2021). However, this model does not provide the flexibility in customizing the atmospheric and topographic parameters. It denotes that this model is more appropriate for larger areas that do not require detailed parameters (Hofierka & Suri, 2002), for instance, for calculating solar energy for large-scale solar farm. Nonetheless, it must be kept in mind that running this model on high-resolution elevation data could significantly increase the computation time.

Hofierka and Suri (2002) developed the *r.sun* module, a fully open-source model implemented in GRASS GIS. It is based on the algorithm used to formulate the European Solar Radiation Atlas by Page et al. (2001). Computation in *r.sun* considers beam (direct), diffuse and ground reflected solar irradiation for given day, latitude, surface and atmospheric conditions (Hofierka et al., 2007). It also uses the Linke atmosphere turbidity factor and surface albedo coefficient to calculate either irradiation or irradiation raster maps. Moreover, the module is able to compute clear-sky solar radiation, i.e. without considering the spatial and temporal variation of clouds (Hofierka, et al., 2007). The model is suitable for modelling large area with complex terrain as the spatial variables can be defined as raster maps (Hofierka & Suri, 2002). It can be considered that this particular model algorithm is especially appropriate for estimating solar radiation in the urban area as the extreme terrain variation impacted by the differences of building heights is likely to exist. The high resolution of topographic data and the variation of building heights in the study area qualifies as complex topography, therefore this algorithm is selected for this thesis.

### Previous research in the solar PV potential modelling

There are multiple studies focus on solar PV potential modelling that has been published. A study by Nguyen and Pearce (2010) published a study titled "*Estimating Potential Photovoltaic Yield with r.sun and the Open Source Geographical Resources Analysis Support System*". As indicated in the title, the study used the *r.sun* module to calculate the solar PV yield, focusing on fourteen counties in Southeastern Ontario. The study incorporated Digital Elevation Model from GTOPO30 and SRTM30, the Linke turbidity factor was derived from the SoDA database, and the surface albedo value was set as a constant value: 0.2. The first step of the computation was executing the *r.sun* module to derive the GHI under clear-sky condition. To obtain solar radiation values under real-sky condition (incorporate the cloud condition), Nguyen and Pearce estimated the clear-sky index ( $K_c$ ) following the formulation by Hofierka and Suri (2002):

$$K_c = G_h / G_{hc} \quad (1)$$

where  $G_h$  is the global radiation under overcast and  $G_{hc}$  is the GHI under clear-sky condition (Hofierka & Suri, 2002). The study performed the  $K_c$  calculation on 99 ground measurement points in the study area. This step followed by interpolating the value to derive the  $K_c$  value for the whole study area. The final step of the study was to multiply the value of clear-sky solar radiation with the interpolated  $K_c$  value. The study concluded that the model had a high handling capacity for the implementation on large-scale photovoltaic system planning (Nguyen & Pearce, 2010).

Another study by Agugiaro et al. (2012), titled "*Solar Radiation Estimation on Building Roofs and Web-Based Solar Cadastre*", estimated solar irradiance on building roofs in the city of Trento in Italy. The study used the *r.sun* module in GRASS GIS as the work environment. The topographical data input was raster-based DSM data from a LiDAR with 1x1m geometric resolution, 15cm height accuracy. The Linke turbidity value derived from secondary data and solar flux value from the in-situ measurement. The cloudiness factor was obtained by comparing the average of 7-year long solar flux observation next to the study area with the calculation result from the *r.sun* module at the same location as the observation point. The result of solar radiation calculation was utilized for reclassification criteria to distinguish the roof surface according to the incoming solar radiation into four categories. The output of the reclassification was exported and visualized in a Web-GIS environment. The study stated that open-source tools had fastened the modelling process and allowed smooth workflow (Agugiaro et al., 2012).

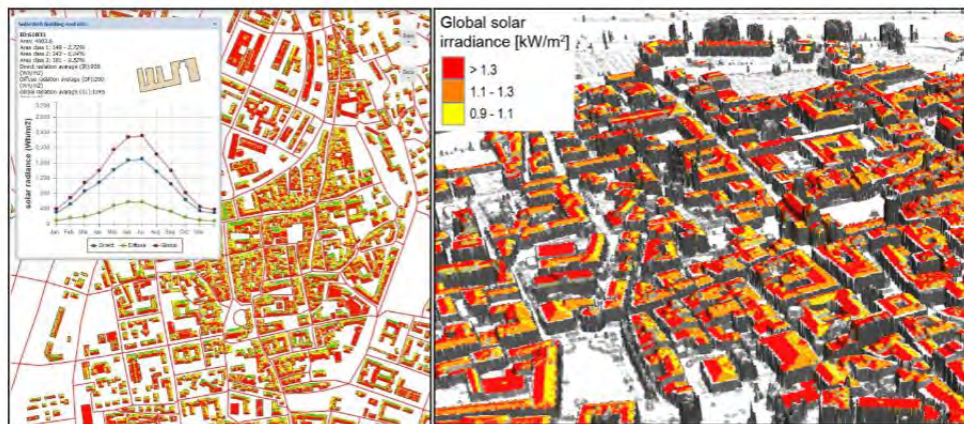


**Figure 7 The interface of the Web-GIS application (Agugiaro et al., 2012)**



A more recent publication by Liang et al. (2020) delivered a more advanced workflow as it extended the *r.sun* model calculation with the 3D principle. It was done by feeding the model with surface slope, aspect and shading, acquired from 3D scene computer graphics methods (Liang et al., 2020). The model also included the shadow casting evaluation using the 360° hemispherical photograph. The output was an open-source software application that can calculate solar radiation on rooftops, facades, and other arbitrary positions, namely Solar3D (Liang et al., 2020).

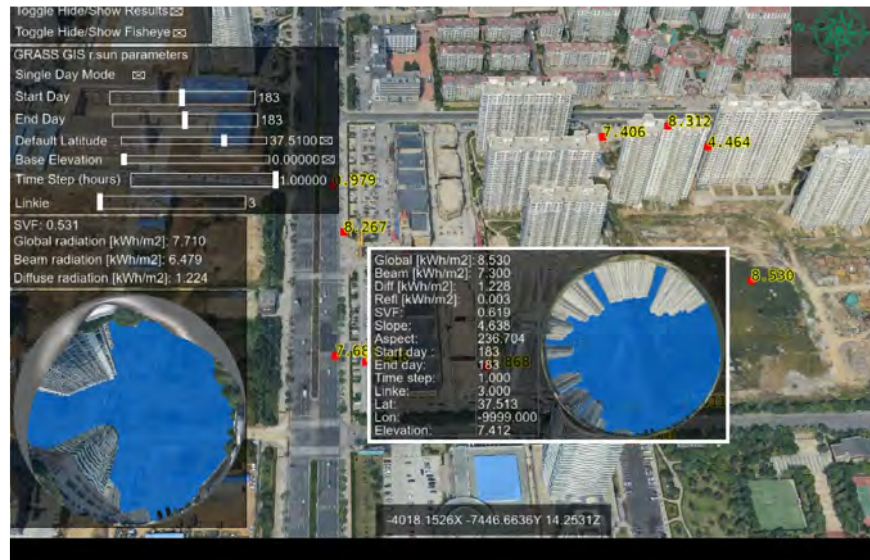


**Figure 8 The output of Solar 3D (Liang et al., 2020)**

### Spatial Data Infrastructure

Spatial data infrastructure (SDI) refers to infrastructure, systems and services that enable the exploration, access, maintenance, dissemination, reuse, and storage of digital geospatial resources (Hu & Li, 2017). SDI could overcome the issue of finding spatial data resources and data redundancy. Better access to geospatial data also encourages the development of new industries that would not have been practicable otherwise (Ralston, 2004). To appropriately function, SDI requires the digital spatial resource and other vital components such as hardware, software, standards, policies, etc.

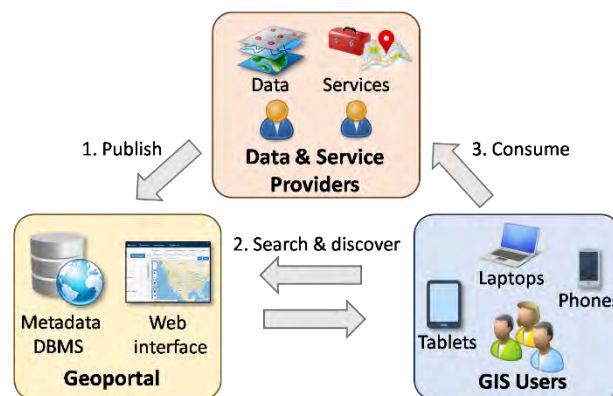


**Figure 9 Key components of an SDI and the publish-find-bind pattern (Hu & Li, 2017)**

The cycle of the SDI operation begins with the publishment of spatial data through the geoportal. The geoportal carries the information and functions as the data-sharing interface and data discovery. SDI should also comprise metadata. The metadata quality is critical to the resource discovery process as it contains the documentation of the data

content. Metadata include essential information in regards to the geospatial resource, such as the description, creation date, license type, spatial references and other things (Hu & Li, 2017). GIS users then will be able to consume the service provided by the data provider by performing a query in the geoportal.

### CityGML

CityGML is one of the solutions to store the building attribute and visualize it in 3D. This solution is also applicable for visualizing the solar PV modelling output since besides it contains the attribute of the solar PV potential, it also includes elevation attribute (derived from point cloud data). According to OGC (2021), CityGML is defined as an XML-based open data model for storing and exchanging virtual 3D city models. The development of CityGML is to standardize the definition of specific entities, characteristic and relations of the 3D city model. Geography Markup Language 3 (GML 3), an extensible international standard for spatial data sharing established by the Open Geospatial Consortium (OGC) and ISO TC211, is used to implement the CityGML (Open Geospatial Consortium, 2021).

The semantic or thematic resources, taxonomies, and aggregations of digital terrain models, locations, vegetation, water bodies, transportation infrastructure, and many more are all represented by CityGML (Kolbe, 2007). Kolbe (2007) also stated that CityGML files are possible to represent in multiple ways for each city object in different Level of Detail (LOD) simultaneously. The example of CityGML visualization of a building in different LOD are the following:

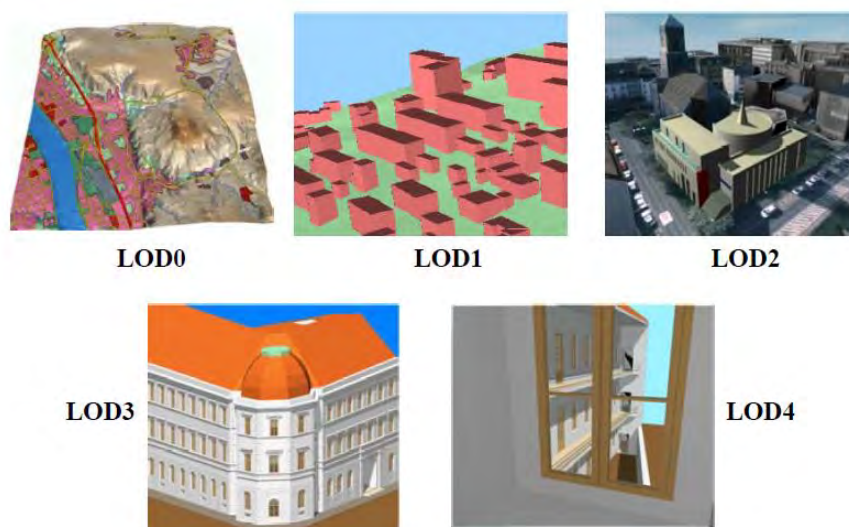


**Figure 10 Different LOD defined in CityGML**

LOD0 is represented as the two and a half dimensional Digital Terrain Model, which will be the base surface of the model. LOD1 comprises buildings with flat roofs. On the contrary, a building has distinct roof designs as well as thematically differentiated surfaces. LOD3 depicts a more detailed model, including architectural features of the model. LOD4 completes a LOD3 model by adding interior structures for 3D objects (Kolbe, 2007).

## 4 MODELLING THE SOLAR PV POTENTIAL

The steps carried out in this stage of work comprise the point cloud data processing and solar radiation computation. The more detailed elaboration of each workflow is the following:

### 4.1 LiDAR Point Cloud Data Processing

The terrain data input for solar radiation computation is the DSM of the Morumbi district generated from LiDAR point cloud data. The downloaded data from the Geosampa web portal were already pre-processed and classified, therefore the steps required to be carried out were merging the point cloud and generate the DSM. The processes were conducted in the PDAL library, which is an open-source library based on C++ for translating and manipulating point cloud data (PDAL, 2021). The library could be installed using Conda and run via Conda shell or Windows terminal.

#### 4.1.1 Merging Point Cloud Data

The point cloud data downloaded from the Geosampa web portal of Morumbi district consists of 55 separate LAZ files. Hence, the point cloud files should be merged into a single LAZ file. PDAL library is able to execute the task through their pipeline, which is represented in JSON format. It should be noted that the whole files that will be merged should be stored in the same directory folder. The pipeline content which was executed for merging Morumbi point cloud data is the following:

```
{
  "pipeline": [
    {
      "type": "readers.las",
      "filename": "./LAZ/*.laz"
    },
    {
      "type": "writers.las",
      "filename": "./LAZ/Morumbi-merged.laz"
    }
  ]
}
```

The PDAL command for executing the pipeline is the following:

```
>> (base) PS C:\Users\Dell> conda activate PDAL
>> (PDAL) PS C:\Users\Dell> pdal pipeline "D:\THESIS\Morumbi\merged-
ptcloud.json"
```

#### 4.1.2 DSM Generation

After merging point cloud data, the next step was the DSM generation. This process was also carried out using a pipeline in the PDAL library. Because the DSM output would be stored in the GeoTIFF format, the pipeline combined PDAL and Geospatial Data Abstraction Library (GDAL), which was already included in the PDAL Conda installation package. The point cloud reader runs under the PDAL library, and the Geotiff writer runs in the GDAL library. The pipeline content is the following:



```
{
  "pipeline": [
    {
      "type": "readers.las",
      "filename": "./LAZ/Morumbi-merged.laz"
    },
    {
      "type": "writers.gdal",
      "filename": "./DSM/dsm-morumbi.tif",
      "resolution": 0.5,
      "output_type": "max"
    }
  ]
}
```

The resolution property indicates the DSM resolution. In this work, the resolution selected for the DSM was 0.5 m. The output\_type property was set to "max", which means the interpolation process is giving the cell the maximum value of all points within the given or default radius (PDAL, 2021). The command for the execution via Conda shell is the following:

```
>> (PDAL) PS C:\Users\Dell> pdal pipeline "D:\THESIS\Morumbi\generatedsm-morumbi.json"
```

In order to reduce the load of computation, the DSM file was clipped using Clip Raster by Mask Layer tool in QGIS.

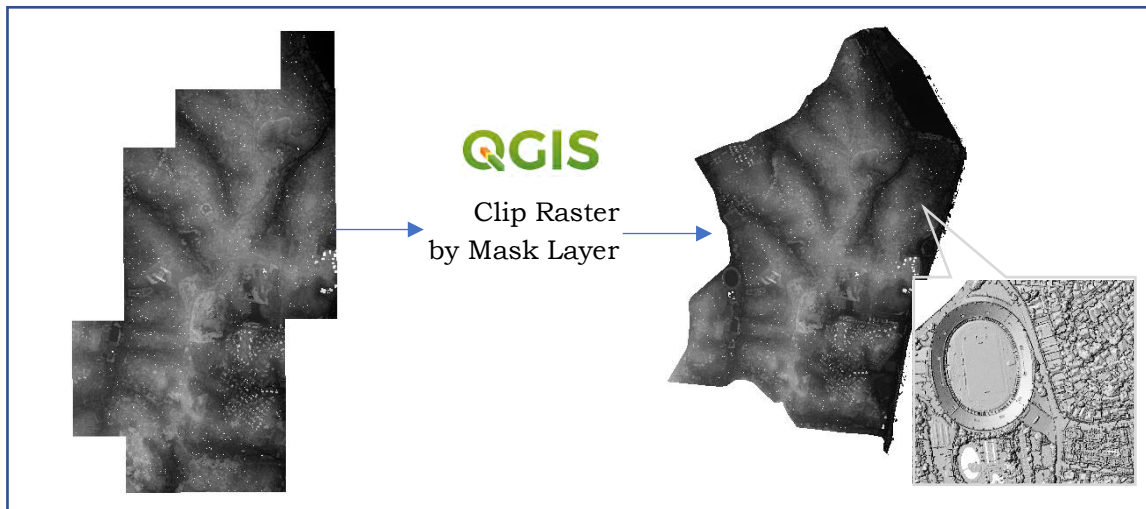


**Figure 11 Clipping in QGIS**

## 4.2 Calculate the Annual Solar Radiation

The second step of the estimation of solar radiation was the calculation of the annual solar radiation itself. The process was carried out in GRASS GIS software using *r.sun* module due to its versatility and performance. Users will have more flexibility to change the parameter input, unlike other solar radiation calculation tools like Solar Radiation Tools in ArcGIS Pro, in which some of the parameters cannot be customized. With regards to the performance, GRASS GIS *r.sun* module was also quite reliable. The tool was able to run in the research area without interruption.

### 4.2.1 Calculate Slope and Aspect

The slope and aspect are essential in solar modelling as those will determine the roof surface orientation and geometry. It influences the amount of solar radiation that will be absorbed. Both slope and aspect maps were generated using *r.slope.aspect* in GRASS GIS. The parameter was set as default. GRASS GIS command that was used in this process is:

```
>>r.slope.aspect      elevation=DSM_MORUMBI@morumbi      slope=slope_morumbi
aspect=aspect_morumbi
```

The building footprint layer from the Geosampa web portal was used for masking. The command was the following:

```
>>r.mask vector=building_footprint@morumbi
```

### 4.2.2 Annual Solar Radiation in Morumbi

The *r.sun* module in GRASS GIS offers two modes, mode 1 calculates radiant flux (power) received by a surface per unit area (irradiance) and mode 2 calculates the solar radiation. The annual solar radiation in this thesis work was calculated using *r.sun*, with mode 2 for the model algorithm. Due to the data availability, the annual solar radiation calculation in this research was using data from the year 2019.

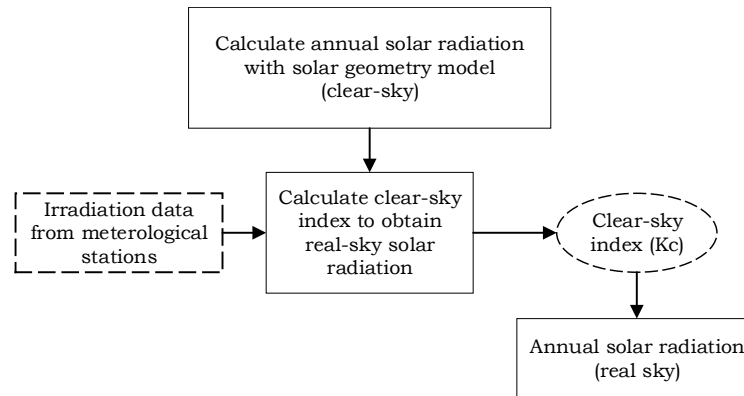


**Figure 12 Solar radiation calculation workflow**

A simple Python script was executed to run the model in a loop for each month. The shadow cast was incorporated, however, the optimal azimuth for the panel arrangement due to shadow casting was not considered in this research. It generated raster layers correspond to each day of the year, with a total of 365 raster layers. The parameters were used for the *r.sun* module input in this research are defined by:

- elevation: the DSM layer of Morumbi district
- slope: slope map
- aspect: aspect map
- horizon\_base: horizon (base name of the horizon map)
- horizon\_step: 30 (unit: degree)
- linke\_value: the Linke turbidity value (January: 3.6, February: 3.5, March: 3.6, April: 3.6, May: 3.15, June: 3.5, July: 3.3, August: 3.5, September: 4.35, October: 4.25, November: 3.75, December: 3.65)
- albedo\_value: the surface albedo value (January: 0.09, February: 0.1, March: 0.09, April: 0.11, May: 0.09, June: 0.08, July: 0.1, August: 0.1, September: 0.12, October: 0.08, November: 0.09, December: 0.09)
- day: day of the year

- step: 0.5 (time step in hours)

Below is the sample of the Python script for calculating solar radiation in January:

```
import os
import sys
import grass.script as gs

gs.run_command('g.region', raster='DSM_MORUMBI')

jan = range(1,32)
for i in jan:
    solrad="janusolrad_morumbi"+ str(i)
    #calculate solar radiation
    gs.run_command("r.sun", elevation = "DSM_MORUMBI",
    aspect="aspect_morumbi", slope= "slope_morumbi",
    linke_value = 3.6, albedo_value = 0.09, horizon_basename=
    "horizon",horizon_step = 30, step = 0.5, glob_rad = solrad,overwrite
    = True, day = i)
```

By aggregating raster layers within the same month using the *r.series* module in GRASS GIS, monthly solar radiation values were obtained. Then, the sum of all layer corresponds to monthly data generated a new raster layer with the total amount of solar radiation within a year.

The annual solar radiation map previously mentioned represents a clear-sky condition. However, in reality, a day with constant clear sky condition is nearly impossible. Sometimes, the solar energy is diffused before it reaches the Earth due to the cloud cover, dust or any other particles which might influence the solar energy absorbance. Thus, the clear-sky index parameter (*K<sub>c</sub>*) is required to obtain the solar radiation value under the real-sky condition. A reverse engineering process was conducted to get the *K<sub>c</sub>* value by performing the calculation based on equation 1. However, a problem occurred due to the unavailability of the meteorological station within the study area. All stations in São Paulo are located outside the Morumbi district, therefore, the process for obtaining the *K<sub>c</sub>* parameter became more complicated and required a longer time. Irradiation data from sensors that are located in the closest proximity from Morumbi were collected for *K<sub>c</sub>* calculation and validation purposes.

Irradiation data from the IAG USP Meteorological Station (23 ° 39' 2" S, 46 ° 37' 19" W) were used for the clear-sky index calculation because it is the nearest weather station from the study area (for a complete table, see attachment 1). The global solar radiation (GHI) data from the sensor was required to obtain the assumption value of real-sky condition GHI in the location. The *r.sun module* was executed again on the location of the meteorological station to get the clear-sky solar radiation values. The result was then divided by the GHI from the ground station for deriving the clear-sky index as follows:

Table 2 Clear-sky index (*K<sub>c</sub>*) value

Month	Kc value
January	0.77
February	0.83
March	0.82
April	0.94

Month	Kc value
May	0.95
June	1.00
July	1.00
August	1.00
September	0.77
October	0.78
November	0.78
December	0.83

The layers aggregated per month were multiplied by the Kc value, resulting in the real-sky solar radiation value. The annual real-sky solar radiation raster layer was generated by summing all 12 layers of real-sky solar radiation, the value is represented in Wh/m<sup>2</sup>.

### Point-based vs Area-based solar radiation calculation

The *r.sun* module in GRASS GIS was fully used in this research for computing solar radiation. However, unlike in ArcGIS Pro, there is no option for calculating solar radiation based on point feature. There are two types of solar radiation calculation in ArcGIS, point-based and raster-based. The first one is applied to a single location on each surface; therefore interpolation process will be minimum. This section examines the differences of both tool types on the exact same location. Six point samples from different buildings with flat roof were selected to identify the result. Both point-based and area-based were executed for the whole year using the same parameter. The result can be seen in Figure 13.

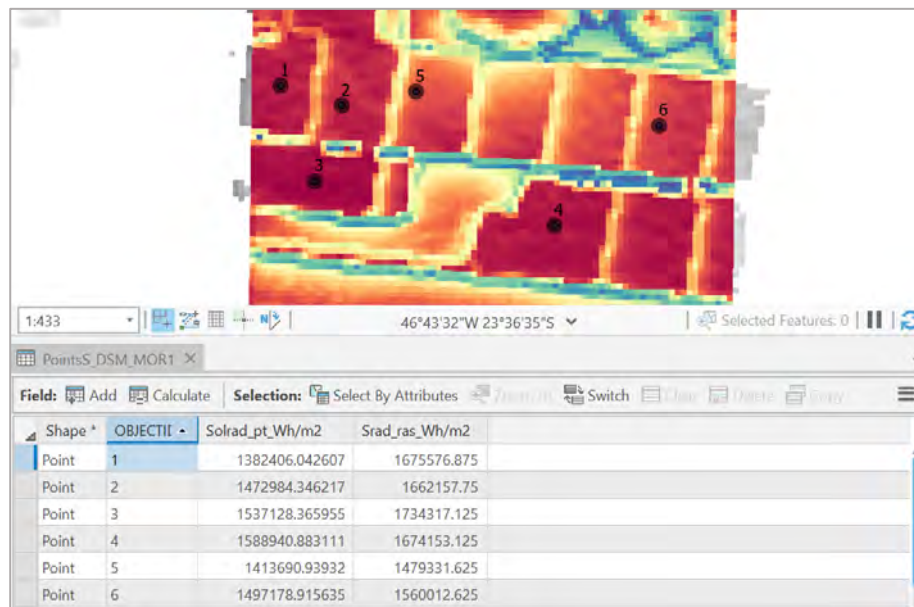


**Figure 13. Point-based vs Raster-based solar radiation calculation**

As indicated in Figure 13, the raster-based calculation results show higher values than the result from the point-based calculation. From the result, it could not be concluded which method was providing the more accurate result. The point-based calculation here has a drawback, as it can only compute a single location. Hence if the

surface has a specific area dimension, the point-based calculation should be carried out multiple time. The larger the surface area, the longer computation time will be required.

### 4.3 Modelling Solar PV Potential

In order to model the solar PV potential in Morumbi, several analyses were required to be conducted. These included identifying the building suitability, calculating the solar power potential on each building rooftop, and other additional analyses such as estimating the PV capacity, installation cost, and assessment of the panel inclination. The steps carried out in this stage are the following:

#### 4.3.1 Building Suitability

Building suitability here means identifying the area of each building that is suitable for solar panel installation. There are some requirements that become the baseline in designing a solar PV system on a rooftop. The National Renewable Energy Laboratory (NREL) in the United States has released a guideline for solar panel installation. The guideline is mentioned within their report in 2013. The NREL released a data set listing roof panels with a slope less than 60 degrees, an orientation ranging from east to west, the number of hours per day in sunlight averaged annually, and the minimum size dimension of 10 m<sup>2</sup> (NREL, 2013). The overall workflow for obtaining building suitability is indicated in Figure 14.

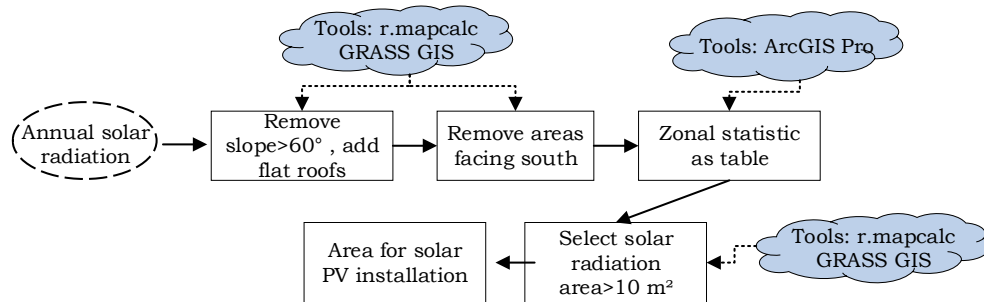


**Figure 14 Building suitability workflow**

The first step was to identify rooftop areas that have less than 60° slopes, as already mentioned in the NREL guideline. The *r.mapcalc* tool in GRASS GIS was run to remove the area with more than 60° slope. The calculation includes adding a conditional expression using the following command:

```
>>r.map.calc                                     expression="yearly_realsky_lowslope"=if(
slope_morumbi@morumbi < 60, yearly_realsky_morumbi@morumbi , null())"
```

This expression involved two layers: the annual solar radiation (*yearly\_realsky\_morumbi*) and the slope layer (*slope\_morumbi*). If an area meets the conditional statement, which is the value from the slope layer (*slope\_morumbi*) is less than 60, the layer will generate a new layer with the solar radiation value from *yearly\_realsky\_morumbi* layer. Meanwhile, the areas that do not meet the conditional statement appeared as *null* or no data. Before eliminating south-facing roof areas, there was one step required to be done, identifying flat roof areas. According to the British National House Building Council (NHBC) standard, roof surface can be categorized as flat if the slope is less than 10° (NHBC, 2020). Following the standard, another conditional expression was run within *r.map.calc* tools in GRASS GIS. The command is the following:

```
>>r.map.calc                                     expression="yearly_realsky_flatslope"=          if(
slope_morumbi@morumbi < 10, yearly_realsky_morumbi@morumbi, null())"
```

The expression above means that if an area has a raster value less than 10, the model will generate a new layer containing the annual solar radiation value. Whereas the area with more than ten as the raster value will be replaced by *null* or no data value. Both layers were multiplied by 1000 to convert the unit to kWh/m<sup>2</sup>.

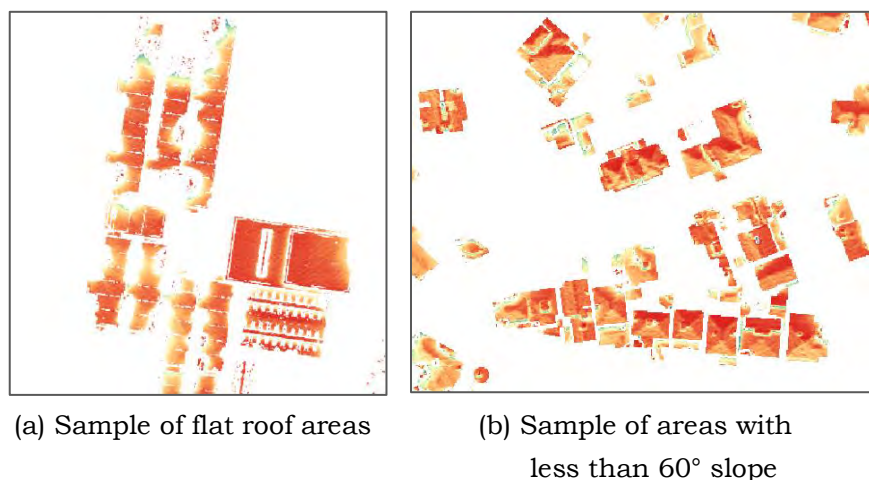


**Figure 15 Result of the *r.map.calc* module for obtaining suitable roof areas**

The second step to identify the area suitable for the solar PV installation was to eliminate the rooftop areas that are facing south. It is due to the location of the study area, which is in the southern hemisphere. The panel will receive more optimum solar energy when it faces the equator. Thus, the areas facing south receive less energy since their heading is facing the opposite direction of the equator. The process was conducted using *r.map.calc* model in GRASS GIS using the following command:

```
>>r.map.calc      expression="yearlyrealsky_northwardfacing"=      if(
aspect_morumbi@morumbi > 225 & aspect_morumbi@morumbi < 315,
yearlyrealsky_flatslope@morumbi , yearlyrealsky_lowslope@morumbi )"
```

In addition to layers generated from slope elimination within the previous step, the aspect layer also played a part in this step. The southward facing areas were obtained from the aspect layer, which has values range from more than 225 and less than 315 (unit in degrees). The areas that met the condition were replaced by the solar radiation layer of the flat surface area that previously generated. Areas that did not meet the condition replaced by the solar radiation layer that the slope criterion has filtered.

The next step of the solar PV potential modelling was conducted in ArcGIS Pro. This step was following the tutorial from (Khanna, 2021). Switching the work environment to ArcGIS Pro was required due to the required tool, Zonal Statistic as Table, which is not available in GRASS GIS. By running the tools in ArcGIS Pro, the mean solar radiation per building could be identified. The result of this analysis was a table that includes the information of the area dimension of the building rooftop suitable for solar panel installation, the average solar radiation on each roof.

OBJECTID *	VALUE	ZONE_CODE	COUNT	AREA	MEAN
1	3161A8831D1900050...	1	646	161.5	1797.975
2	3161A8831D19000D0...	2	58	14.5	1092.591
3	3161A8831D1900100...	3	709	177.25	1641.291
4	3161A8831D1900080...	4	100	25	1435.383
5	3161A8831D19000D0...	5	1116	279	1633.51
6	3161A8831D1900050...	6	205	51.25	1481.472
7	3161A8831D19000D0...	7	614	153.5	1968.782

**Figure 16 Sample of Zonal Statistic as Table result in ArcGIS Pro**

The last part of this stage of work was removing the building polygons, which have an area dimension of less than 10 m<sup>2</sup>. This process was simply done by performing a *join* between the table from the Zonal Statistics as Table result with the building footprint layer. Then, by executing *Select by Attribute* tools, buildings with less than 10 m<sup>2</sup> area were filtered out. The result of this process was the building layer suitable for the PV installation.

### 4.3.2 Calculate Rooftop PV Potential Per Building

A simple calculation using *field calculator* tools in ArcGIS Pro was used to compute the rooftop PV potential on each building. The energy generated was obtained using the following formula (EPA, 2021):

$$E = A \cdot r \cdot H \cdot PR \quad (2)$$

- A = Total solar panel Area (m<sup>2</sup>)
- r = Solar panel efficiency (%)
- H = Annual average solar radiation
- PR = Performance ratio, the coefficient for losses
- E = Energy (kWh)

Based on the report from Instituto Ideal and AHK RIO (2019), Brazil's average solar panel efficiency is 15%. The performance ratio ranges from 0.6 to 0.9, depending on the solar panel material (Zdyb & Gulkowski, 2020). In this research, 0.8 was assumed as the performance ratio for the input of the energy calculation.

First of all, the total solar radiation received by each building was calculated by multiplying the *AREA* field and *MEAN* field. Then it had been multiplied by 0.15 (efficiency) and 0.8 (performance ratio). The result was then divided by 1000 to get the energy in MWh/year. It should be noted that in this research, the storage system using battery and inverter is not considered.

### 4.3.3 Additional Analyses

#### PV Capacity

The PV capacity was derived by following the rule of thumb of the PV system design. One kWp (kilowatt peak) PV system requires a 10 m<sup>2</sup> area (Homescape, 2019). Therefore, by dividing the area of the suitable building by 10, the PV capacity attribute values could be obtained. Again, the calculation process was carried out using *field calculator* tools in ArcGIS Pro.

#### Installation Cost

The installation cost was simply calculated to provide the estimated cost for the PV system installation to the building owner. The average cost of PV installation in Brazil was provided by Instituto Ideal and AHK RIO (2019). One kWp PV system costs 6,460 Brazilian Real (BRL). The PV Capacity field was multiplied by 6,460 to get the PV installation cost per building by running the field calculator tools.

#### CO<sub>2</sub> emission savings

As previously mentioned in the introduction, the primary purpose of solar energy utilization is to reduce the amount of CO<sub>2</sub> emission. Thus, the CO<sub>2</sub> emission savings was calculated in this research. The highest portion of fossil energy resource for electricity



generation in Brazil is fuel oil (IEA, 2018). Thus, the CO<sub>2</sub> emission savings here were assumed by calculating the emission from fuel oil for electricity generation, which can be reduced if the fuel is switched to solar energy. The average CO<sub>2</sub> emitted by fuel oil for electricity generation is 280 kgCO<sub>2</sub>e per MWh (Quaschnig, 2016). By multiplying the value with the solar energy generated using *field calculator* tools, the amount of CO<sub>2</sub> emission savings per building could be identified.

### Assessment on the impact of panel inclination adjustment

The amount of solar energy that the PV panel can receive is very much dependent on the sun position. Hence, changing the arrangement of the PV panel can increase or decrease solar radiation absorption. The arrangement can be altered on the panel inclination and heading. Since the panel position for non-flat roof surface (gabled, pitched, dome) is fixed due to the formation and roof slope, the alteration can only be done for roofs with a flat surface. This optimization analysis was carried out once again using the *r.sun module* in GRASS GIS. The workflow for this analysis was:

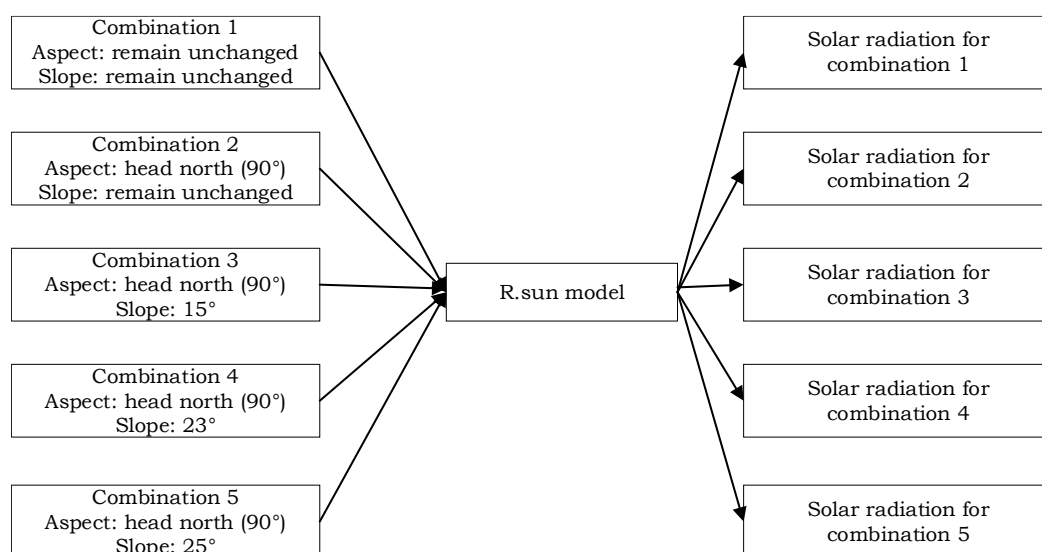


**Figure 17 Assessment workflow**

The step was similar to the solar radiation modelling in section 4.2.2, with the modification of the slope and aspect input layer. The slope layer was assumed as the panel inclination, modified to 15°, 23°, and 25°. 15° and 25° are the standard inclination option in solar PV installation, whereas 23° is the latitude of the study area. In theory, the most optimum panel inclination angle is equal to the local geographic latitude (Hailu & Fung, 2019). The option for the heading was unmodified and modified by northward facing (90°). As the sun position changes are more depictable using the seasonal period, the model was run for selected days within a month of each season (winter, summer, autumn, spring). The dates used for this analysis are defined by:

- Winter: June 14 – June 18
- Summer: December 13 – December 18
- Spring: September 13 – December 17
- Autumn: March 22 – March 26

The *r.sun module* was run for each parameter combination. The combination that was resulting the highest solar radiation was considered the most optimum panel configuration.

## 5 VISUALIZATION

This chapter highlights the steps that had been conducted for the visualization process. As already stated in the objective, the solar PV potential in Morumbi is visualized within an integrated spatial data infrastructure. This visualization aims to support potential users, i.e. the government, citizens, and solar energy engineers in the study area, to identify solar photovoltaic potential. The spatial data infrastructure is selected as the visualization framework to facilitate data transferability and interactivity. In order to achieve the objective, a web-map application and CityGML model were generated during this research. Steps that had been carried out for creating the web-map application of work include building a spatial database, set up the server, and web-map application deployment, which are shown on the workflow below:

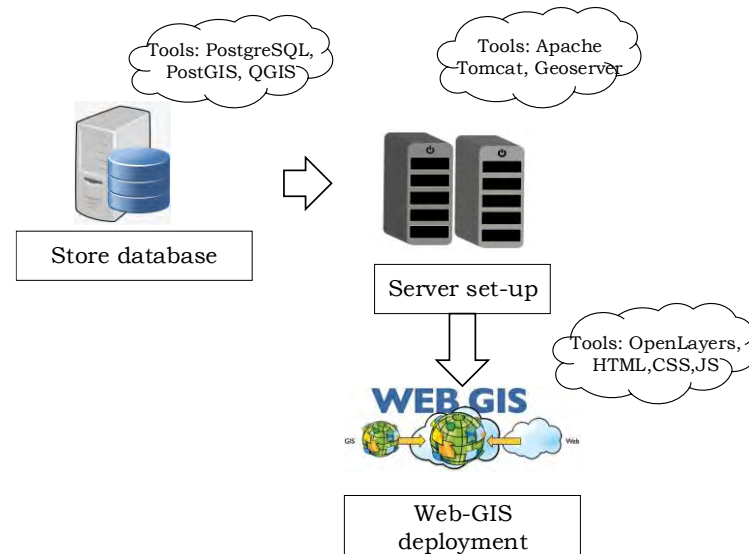


**Figure 18 Web-map application deployment workflow**

### 5.1 Building a spatial database

A spatial database is required for managing layers that will be displayed on the web-map application. In this research, the spatial database was deployed using an integration of PostgreSQL and PostGIS database. The PostgreSQL version that was used in this research is version 12. The database was created in PgAdmin 4, the database administration tool that is included within PostgreSQL installation. First, a new server named *solar* was created in PgAdmin. Due to the unavailability of an allocated live server, the server was created within a local host.

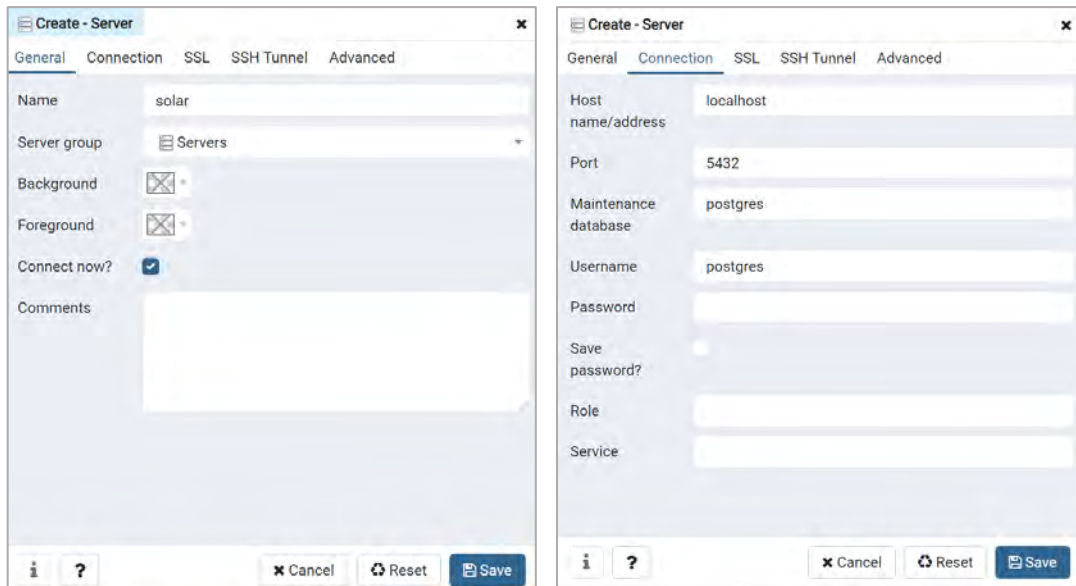


**Figure 19 Create PostgreSQL server**

The next step was to create the database. Here the database is called *solar\_pot* with the username is *postgres*. The command for the database creation is the following:

```
CREATE DATABASE solar_pot
WITH
OWNER = postgres
ENCODING = 'UTF8'
LC_COLLATE = 'English_United States.1252'
LC_CTYPE = 'English_United States.1252'
TABLESPACE = pg_default
CONNECTION LIMIT = -1;
```

PostgreSQL does not support spatial feature storage. Hence, the PostGIS extension should be installed within the database. The installation could be done using PgAdmin using SQL command:

```
CREATE EXTENSION postgis
SCHEMA public
VERSION "3.1.1";
```

The process for uploading the layer to the database was done through QGIS using *DB Management* tools. This tool was also used to set the primary key and add a geometry column in the table (*geom*). The coordinate system was changed from EPSG:31983 to EPSG:4336 to avoid projection and coordinate system issues later during front-end programming for the web-map application.

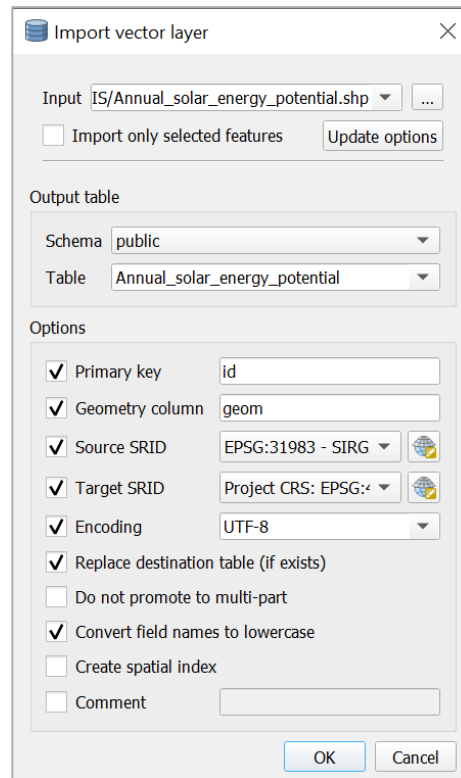


**Figure 20 DB Management tools setting in QGIS**

The database contains four tables. The database design includes each table and columns is indicated in Figure 21. The *Annual\_solar\_energy\_potential* table, which contains the solar PV potential information, was inherited from the building footprint table. The same condition applies to the *Unsuitable\_building\_for\_PV* table. The *favela\_morumbi* layer is an independent layer that contains the information of the slum area in Morumbi.

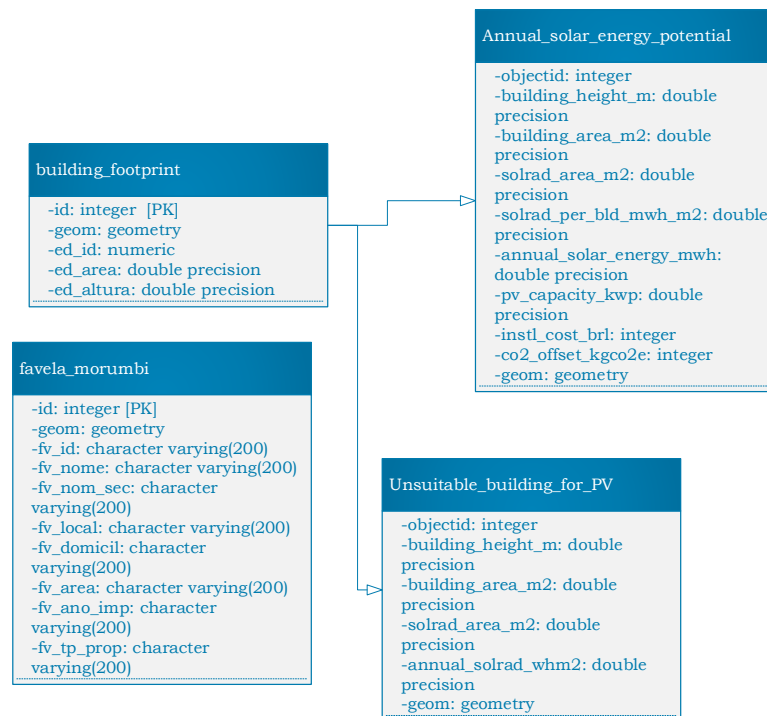


**Figure 21 Database design**

## 5.2 Setup a server

For displaying the layer on the web-map application, a server needs to be set up. It is required to handle the data transaction and communication between the client and the database. Apache Tomcat 9.0 was used for a local server and servlet engine. In this work, the Apache Tomcat server was installed locally within port:8081 in the Department of Geoinformatics, Palacky University Olomouc. Geoserver was installed by copying the web archive installation package to the *webapps* directory of Apache Tomcat. Geoserver 2.8 runs within the servlet engine to render the vector and raster layers that adhere to the OGC standard.

Tomcat Web Application Manager

Message:

OK

Manager

List Applications

HTML Manager Help

Manager Help

Server Status

Applications

Path	Version	Display Name	Running	Sessions	Commands
/	None specified	Welcome to Tomcat	true	0	<div>Start Stop Reload Undeploy</div> <div>Expire sessions with idle ≥ 30 minutes</div>
/docs	None specified	Tomcat Documentation	true	0	<div>Start Stop Reload Undeploy</div> <div>Expire sessions with idle ≥ 30 minutes</div>
/examples	None specified	Servlet and JSP Examples	true	0	<div>Start Stop Reload Undeploy</div> <div>Expire sessions with idle ≥ 30 minutes</div>
/geoserver	None specified	GeoServer	true	0	<div>Start Stop Reload Undeploy</div> <div>Expire sessions with idle ≥ 30 minutes</div>
/host-manager	None specified	Tomcat Host Manager Application	true	0	<div>Start Stop Reload Undeploy</div> <div>Expire sessions with idle ≥ 30 minutes</div>
/manager	None specified	Tomcat Manager Application	true	1	<div>Start Stop Reload Undeploy</div> <div>Expire sessions with idle ≥ 30 minutes</div>
/webgis	None specified		true	0	<div>Start Stop Reload Undeploy</div> <div>Expire sessions with idle ≥ 30 minutes</div>

**Figure 22 Apache Tomcat application manager**

Afterwards, the Geoserver interface was accessed via the web browser to perform the data rendering and publishing. The vector layers available on the PostgreSQL database was published as Web Map Service (WMS) and Web Feature Service (WFS), while the raster layer was published as WMS. The first step for publishing the layers is to create a new workspace to store the layers. Then, within the workspace, a Geoserver store should be created to facilitate the communication between the server and the database. The vector data stored in the PostgreSQL database can be called via the PostGIS database data type option, where the raster layer can be accessed by selecting the GeoTIFF raster data source option. Within the store setting interface, the server admin should add the connection details to the database. Once the store configuration is saved, the layer can be published using the *layer – add new layer* option.

Layers						
Manage the layers being published by GeoServer						
<a href="#">Add a new layer</a> <a href="#">Remove selected layers</a>						
<< < 1 > >> Results 1 to 6 (out of 6 matches from 40 items) <input type="text" value="solar"/> <a href="#">Clear</a>						
<input type="checkbox"/>	Type	Title	Name	Store	Enabled	Native SRS
<input type="checkbox"/>		Annual_solar_PV_potential_MWh	solar_pot:Annual_solar_PV_potential_MWh	Annual_solar_PV_potential	✓	EPSG:4326
<input type="checkbox"/>		Annual_solar_radiation_kWh_m2	solar_pot:Annual_solar_radiation_kWh_m2	Annual_solar_radiation_kWh_m2	✓	EPSG:4326
<input type="checkbox"/>		Morumbi_boundary	solar_pot:Morumbi_boundary	Annual_solar_PV_potential	✓	EPSG:4326
<input type="checkbox"/>		Unsuitable_building_for_PV	solar_pot:Unsuitable_building_for_PV	Annual_solar_PV_potential	✓	EPSG:4326
<input type="checkbox"/>		building_footprint	solar_pot:building_footprint	Annual_solar_PV_potential	✓	EPSG:4326
<input type="checkbox"/>		favela_morumbi	solar_pot:favela_morumbi	Annual_solar_PV_potential	✓	EPSG:4326
<< < 1 > >> Results 1 to 6 (out of 6 matches from 40 items)						

**Figure 23 Published layers on Geoserver**

Within Geoserver, the layer symbology can be customized according to the user preference. The symbology style is based on Styled Layer Descriptor (SLD), an OGC-specified XML schema to describe the symbology of raster and vector layer (Geoserver, 2021). The custom styling example of the annual solar PV potential layer is the following:

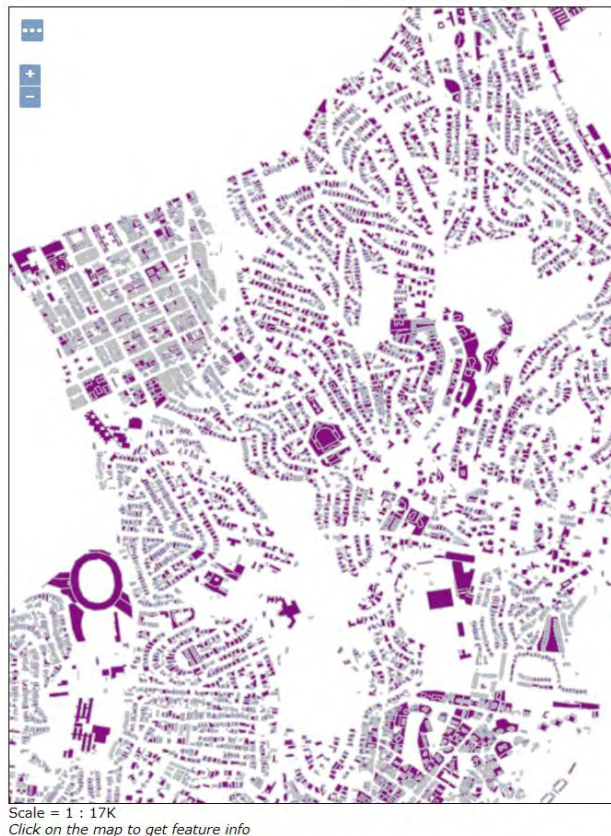
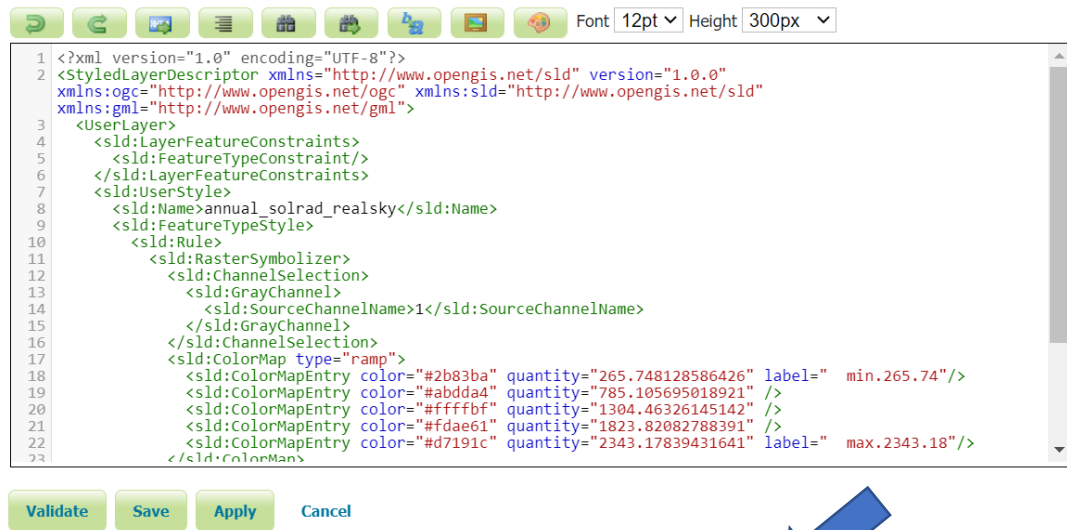


**Figure 24 SLD document snippet and the preview of the annual solar PV potential layer**

The user is also able to alter the WMS and WFS feature info, which indicates the attribute values of a layer. The attribute shown in the feature info can be filtered according to user needs. By creating a freemarker template (.ftl), users can modify the *GetFeatureInfo* output. The template can generate the output in HTML and GeoJSON format (Geoserver, 2021).



Below is an example of an HTML customized template of the annual solar PV potential layer:

```

1 <style>
2 html,body {
3   text-align: left;
4   font-size: 90%;
5 }
6 .container dt,.container dd {
7   width:auto !important;
8   margin-left:auto !important;
9   display:inline-block !important;
10 }
11 </style>
12 <#list features as feature>
13 <dl class="row">
14   <dt class="col-sm-6 text-left">Object id:</dt>
15   <dd class="col-sm-9 text-left">${feature.objectid.value}</dd>
16
17   <dt class="col-sm-6 text-left">PV area (m2):</dt>
18   <dd class="col-sm-9 text-left">${feature.solrad_area_m2.value}</dd>
19
20   <dt class="col-sm-6 text-left">Irradiation:</dt>
21   <dd class="col-sm-9 text-left">${feature.solrad_per_bld_mwh_m2.value} (MWh/m2/year)</dd>
22
23   <dt class="col-sm-6 text-left">Annual solar energy:</dt>
24   <dd class="col-sm-9 text-left">${feature.annual_solar_energy_mwh.value} (MWh)</dd>
25
26   <dt class="col-sm-6 text-left">PV capacity:</dt>
27   <dd class="col-sm-9 text-left">${feature.pv_capacity_kwp.value} (kWp)</dd>
28
29   <dt class="col-sm-6 text-left">Installation cost:</dt>
30   <dd class="col-sm-9 text-left">${feature.instl_cost_brl.value} BRL</dd>
31
32   <dt class="col-sm-6 text-left">CO2 offset:</dt>
33   <dd class="col-sm-9 text-left">${feature.co2_offset_kgco2e.value} (kgco2e)</dd>
34 </dl>
35 </#list>

```

(a) Freemarker template file content



Scale = 1 : 17K

Object id:  
4633  
PV area (m2):  
2735.75  
Irradiation:  
5527.95 (MWh/m2/year)  
Annual solar energy:  
663.35 (MWh)  
PV capacity:  
273.58 (kWp)  
Installation cost:  
1767294 BRL  
CO2 offset:  
185739 (kgco2e)

(b) *GetFeatureInfo* output

**Figure 25 *GetFeatureInfo* customization**

## 5.3 Web-map application deployment

For displaying the client-side interface, a web-map application has been deployed. The tools used for creating the web-map application was OpenLayers 6.5.0. OpenLayers was



selected due to its versatility and ability to add various customizable elements to the webpage. The workflow scheme of the overall data transaction is the following:

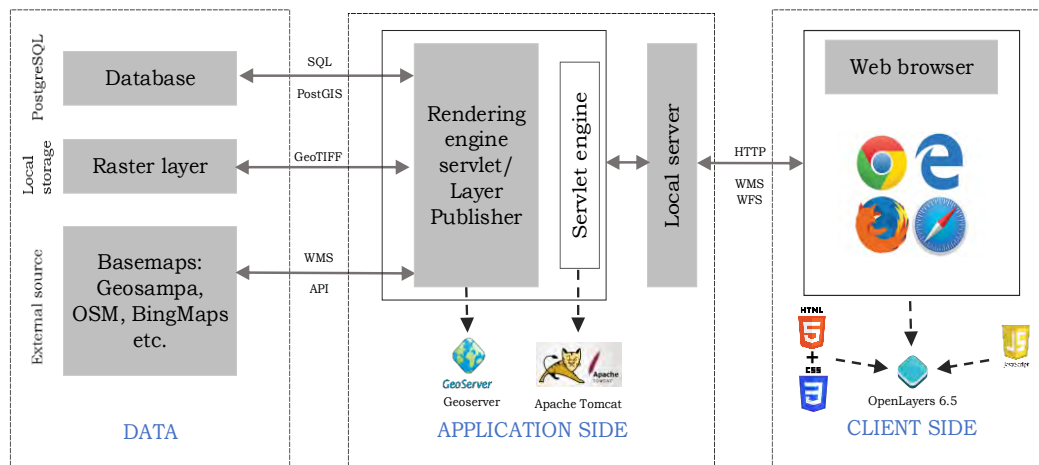


**Figure 26 Data transaction workflow**

The displayed layers on the web-map application are in WMS format. The principle is the WMS will be rendered on the web browser by calling the server to retrieve the layer from Geoserver. After creating the HTML layout and adding styling elements via CSS, the layer is called to be displayed on the web-map application using JavaScript syntaxes. A code snippet example for displaying the annual solar energy potential on the web-map application is the following:

```

var overlays = new ol.layer.Group({
  'title': 'Layer selection',
  layers: [
    new ol.layer.Image({
      title: 'Annual_solar_energy_potential_MWh',
      source: new ol.source.ImageWMS({
        url: 'http://158.194.129.29:8081/geoserver/solar_pot/wms',
        params: {'LAYERS':
          'solar_pot:Annual_solar_energy_potential_MWh',
          ratio: 1,
          serverType: 'geoserver'}})
    })
  ],
});

```

The web-map application is equipped with some additional functions. The additional functions were featured by adding some dynamic JavaScript elements to the source code. The functions were presented by incorporating OpenLayers library with *ol-ext* extension by Viglino (2021). The design and functionalities selection were adapted from K. Choudary (personal communication, April 11, 2021). The functions summary include:

- Layer selection and base map options
- Toggle fullscreen, zoom in-out, zoom extent, overview map
- Geocoding
- Measurement
- Pop-up options
- Adding additional WMS layers
- Query tool and Select by Draw, Zoom to selected attributes from the query

## 5.4 Store the building model in CityGML format

Since the topographical data input for the solar PV potential analysis were created from point cloud data, 3D building models of the study area can be generated. The author decided to store the building in CityGML format because it is an OGC compliant standard specifics for the 3D city model. The file is based on XML, which is able to function as storage and exchange media of city models (Open Geospatial Consortium, 2021). The process for generating the CityGML model was done using the FME Desktop - Safe software. It is software for a data integration platform. The data manipulation capabilities of FME can be used to transform data, convert file formats, or do both at the same time (Safe Software, 2021). The interface of the software is synonymous with the ModelBuilder feature in ArcGIS Pro or ArcMap. Each geoprocessing tool is called a *transformer*.

The CityGML generation process in the FME workspace begins with clipping the point cloud data using the building footprint. Then, a Digital Terrain Model (DTM) was created to obtain the ground elevation as the base height of the building. By running the *SurfaceDraper* transformer, the building footprint layer was overlaid with the DTM to extract the ground elevation to be stored as the *base\_height* attribute. The building height was calculated by subtracting the median elevation of each building geometry from the point cloud data with the *base height*. The next step was the building extrusion. It aims to create 3D visualization from a 2D vector layer, which is the building footprint, and extrude it based on the building heights derived from 3D point cloud data using *3DForcer* and *Extruder* transformer. Afterwards, the translation process to CityGML was done by adding the CityGML feature class reader to the workspace.

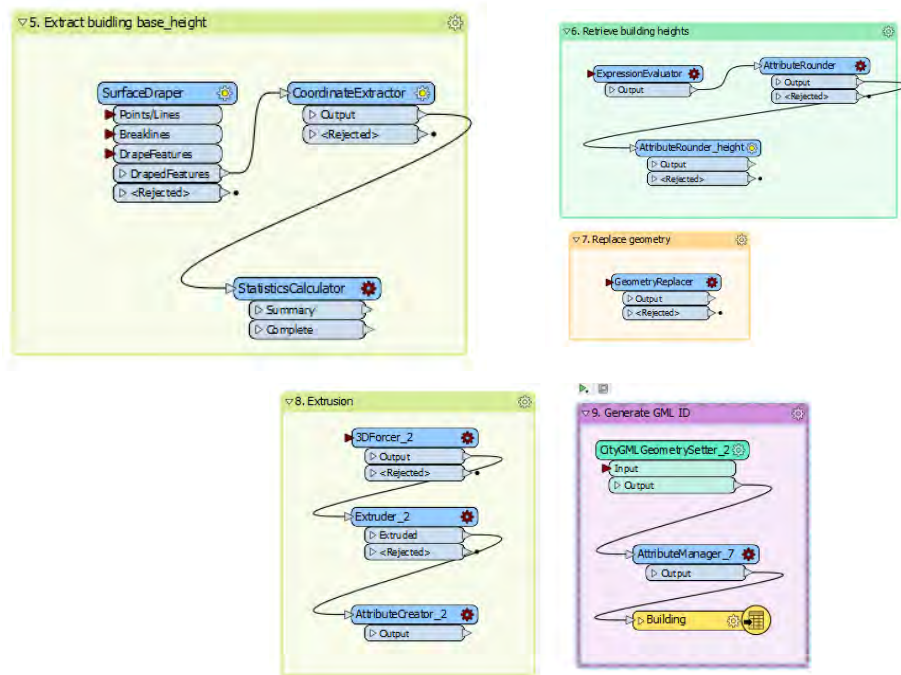


**Figure 27 Key processes in CityGML generation**

The result of this step was a CityGML document that includes the building model information, such as the level of detail and GML id. The XML-based document also consists of solar PV potential attributes, similar to the annual solar PV potential layer.

## 6 RESULTS

This chapter elaborates the result that has mentioned in the previous chapter. It is divided into two parts, the analysis and visualization result. The analysis part consists of solar radiation trends in the study area, the building suitability, the total generated solar energy in the study area, the total CO<sub>2</sub> emission savings, and the impact of the panel inclination adjustment in the study area. The visualization part shows the interface of the web-map application and the result of the building model in the CityGML format.

### 6.1 Analysis

#### Annual solar radiation in Morumbi

The amount of annual solar radiation in Morumbi was derived from the modelling process using the *r.sun module* in GRASS GIS. It is presented in a raster file with a resolution of 0.5 m, with each pixel grid represents the solar radiation value. The maximum, minimum, and mean annual solar radiation in Morumbi can be identified from the raster data.

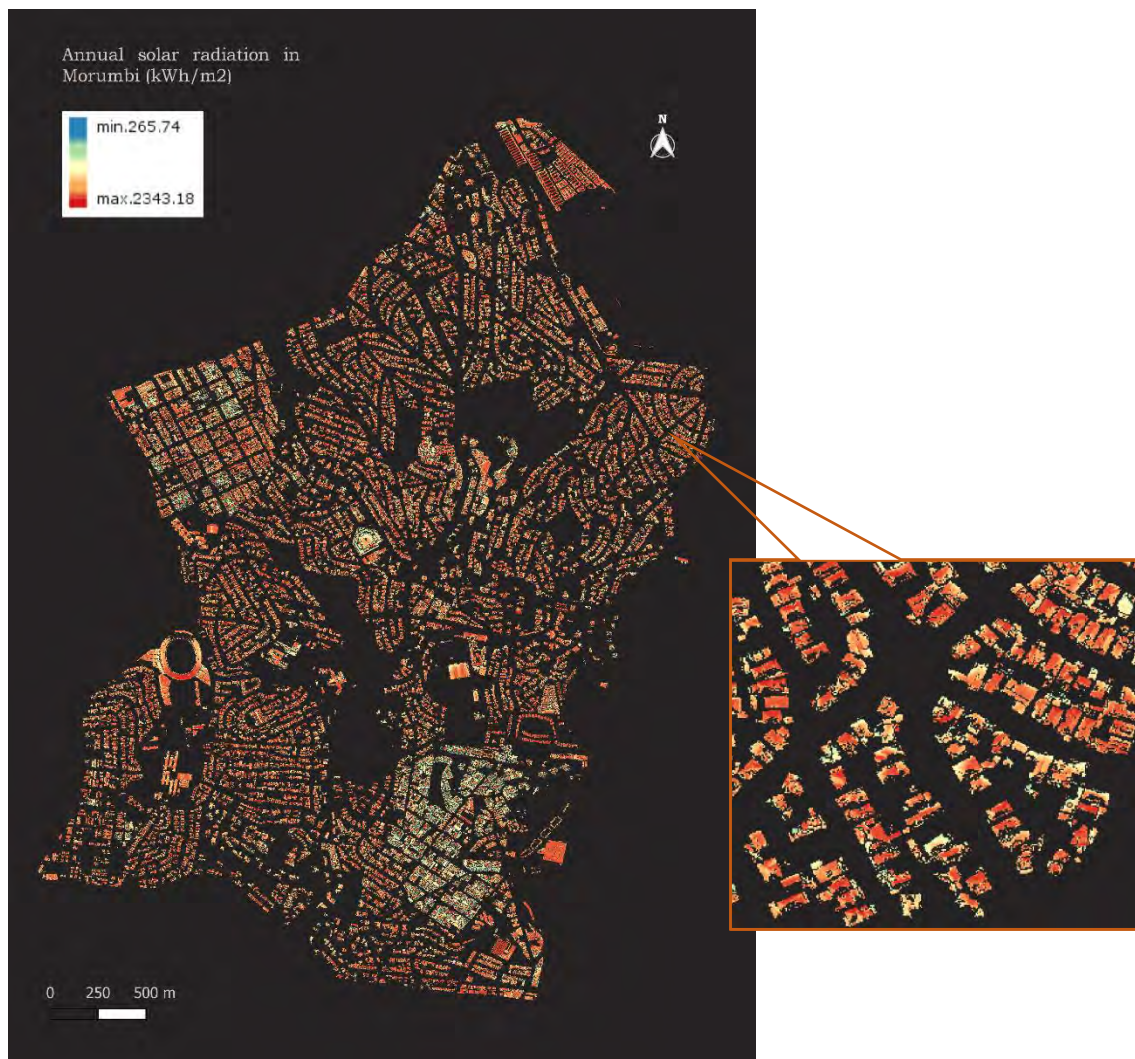


Figure 28 Annual solar radiation in Morumbi

The amount of solar radiation in Morumbi varies, depending on the orientation and slope of the roof surface and the shadow casting from the surroundings. It must be kept in mind that in this analysis, it is assumed that the panel installation would be parallel to the roof surface. Using *raster layer statistics* tools in QGIS, it can be identified that the maximum annual solar radiation in the Morumbi area is 2,343.18 kWh/m<sup>2</sup>, the minimum is 265.74 kWh/m<sup>2</sup>, and the mean is 1,778.54 kWh/m<sup>2</sup>. In order to provide better information on the GHI distribution in Morumbi, the area distribution of the GHI interval had been calculated. The GHI was reclassified into five classes, with each class represents the GHI interval. The step was carried out by executing the *Reclassification* tool in ArcGIS Pro, which provided a vector file as the output. The vector file contains the information of the number of pixel of each class inside the attribute table (COUNT). The total area of each class then derived by multiplying the number of pixels with 0.25 (the area dimension of one pixel) and 0.0001 to convert the unit to hectares.

Table 3 Area distribution of the annual GHI

Annual GHI (kWh/m <sup>2</sup> )	Total area (ha)
0-500	1
500-1,000	10
1,000-1,500	33
1,500-2,000	89
2,000-2,500	73

The result can be seen in Table 3 and Figure 29. Pixels with a solar radiation value from 1,500 to 2,000 kWh/m<sup>2</sup> have the highest area distribution.

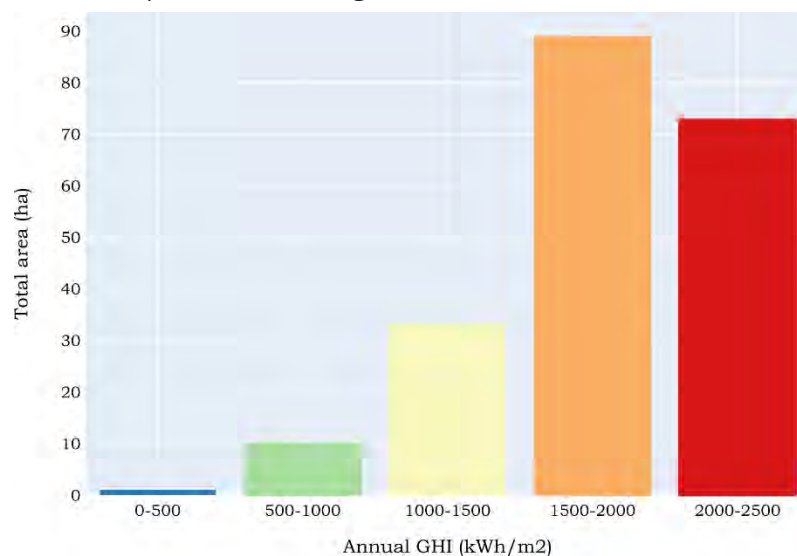


**Figure 29 Raster histogram of the annual solar radiation**

By dividing the mean solar radiation by 365, the daily solar radiation or GHI can be estimated. The computed average daily GHI in Morumbi is 4.87 kWh/m<sup>2</sup>. The result can be compared with the average daily GHI from other regions in the southern hemisphere. Table 4 compares the GHI of Morumbi with countries with equivalent latitude and countries in the southern hemisphere. The country's daily GHI data and estimated PV output were derived from Energy Sector Management Assistance Program (ESMAP) (ESMAP, 2020). The daily GHI of Morumbi is lower than most of the regions with the equivalent latitude, including the average daily GHI in Brazil and slightly higher than the



daily GHI in Morumbi. Nevertheless, the daily GHI in Morumbi is higher than the lowest daily solar radiation within Brazil. It can be concluded that there is a great potential for the development of solar PV in Morumbi.

Table 4 Comparison of daily GHI

Region	Daily GHI (kWh/m <sup>2</sup> )
South Africa	5.6
Paraguay	5.0
Uruguay	4.7
Australia	5.3
Brazil (average)	5.2
Brazil (minimum)	4.1
Morumbi	4.78

As specified in section 4.2.2, the initial result of the model is 365 raster files correspond to each day of the year (Julian date). Thus, the trend of solar radiation can be identified. Figure 30 indicates the diurnal solar radiation trend in a real-sky condition and a clear-sky condition (before multiplied by the clear-sky index), which obtained by calculating the mean of daily solar radiation data within a month. For example, to obtain monthly solar radiation in January, the mean of layers from day 01 to day 31 was calculated.

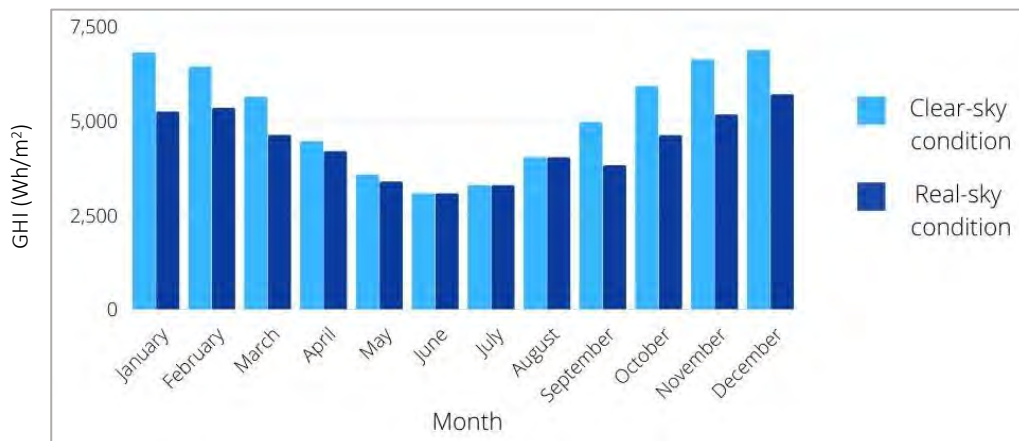


**Figure 30 Monthly diurnal GHI trend in Morumbi**

December is the month with the highest solar radiation value. In December, the estimated solar radiation under clear-sky and real-sky conditions are 6,865.49 Wh/m<sup>2</sup> and 5,698.35 Wh/m<sup>2</sup>. June is the month with the lowest solar radiation. The estimated solar radiation under the clear-sky condition and the real-sky condition in June is 3,069.07 Wh/m<sup>2</sup>. The value of both sky conditions are the same as the clear-sky index value is 1.0. The monthly trend of solar radiation seems to correspond with the seasonal change, as the lowest monthly solar radiation is in the winter season, December, a month in the winter season, receives the highest solar radiation.

The chart within Figure 30 shows significant gaps between the clear-sky and the real-sky condition in data within the end of spring and during the summer season (October to February). It is due to the clear-sky index of both months are the lowest. The author tried to identify the correlation between the significant gaps of GHI values with the cloud

fraction during the specific time period. Research from Yamasoe et al. (2016) provides the information of cloud fraction in São Paulo city, which can be seen in Figure 31.

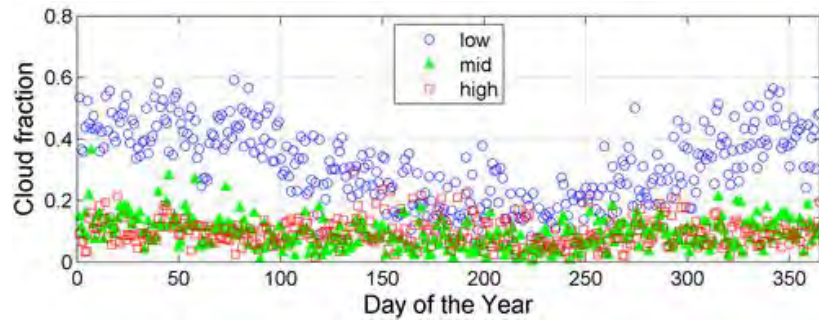


**Figure 31 Daily mean value of the cloud fraction associated with the presence of clouds in bottom multilayers, based on hourly observations performed from 7:00 A.M. to 6:00 P.M (Yamasoe et al., 2016)**

It can be seen from Figure 31 that the variation of cloud fraction is showing its highest trend on day 1-50 (January-February) and day 300-365 (October-December). Therefore, it can be concluded that the variation of the clear-sky index value is highly influenced by the cloud fraction. However, more factors should also be taken into account in terms of atmospheric attenuation, such as dust, aerosol, etc. Moreover, the time step parameter should be taken into account when calculating the solar radiation value. The aggregation of each atmospheric parameter would affect the prediction; therefore, selecting the time-step parameter should be in line with the temporal resolution of the atmospheric parameter. For example, in calculating diurnal solar radiation, a smaller time step should be considered since the atmospheric attenuation factor varies over time.

### Rooftop PV potential

One of the objectives of this research is to assess the solar PV potential of each building rooftop within the study area. By identifying the building suitability (chapter 4.3.1), the total annual energy yield from the rooftop PV system in Morumbi can be estimated. The number of suitable buildings for rooftop PV installation is 10,894, of the total of 11,780 buildings (slums are not taken into account). It indicates that around 92% of buildings in Morumbi are feasible for rooftop solar PV installation.

objectid	building_height_m	building_area_m2	solrad_area_m2	rad_per_bld_mwh	annual_solar_energy_mwh
10885	11758	3	57.55	12.75	13.86
10886	11759	6	336.47	220.75	342.45
10887	11760	6	155.64	145	276.88
10888	11761	8	49.87	19	23.3
10889	11763	6	308.34	264.5	482.14
10890	11765	14	223.08	155.75	302.79
10891	11766	7	42.15	42	74.72
10892	11767	3	182.34	84	91.8
10893	11768	26	68.31	46.5	83.03
10894	11769	6	167.69	133	259.12

objectid	building_height_m	building_area_m2	solrad_area_m2	annual_solar_energy_mwh
877	8494	5	16.2686126156	2
878	337	3	26.4225999977	8
879	8387	3	8.33791114176	0.25
880	316	3	41.6966716718	2.75
881	8341	3	12.3393294593	8.5
882	8332	7	29.7530682172	1.75
883	8443	4	17.9124820968	6.5
884	8440	4	16.8557259732	4.75
885	8416	3	15.1273087869	9.75
886	8397	6	16.1414999997	1

**Figure 32 Number of features (buildings)**

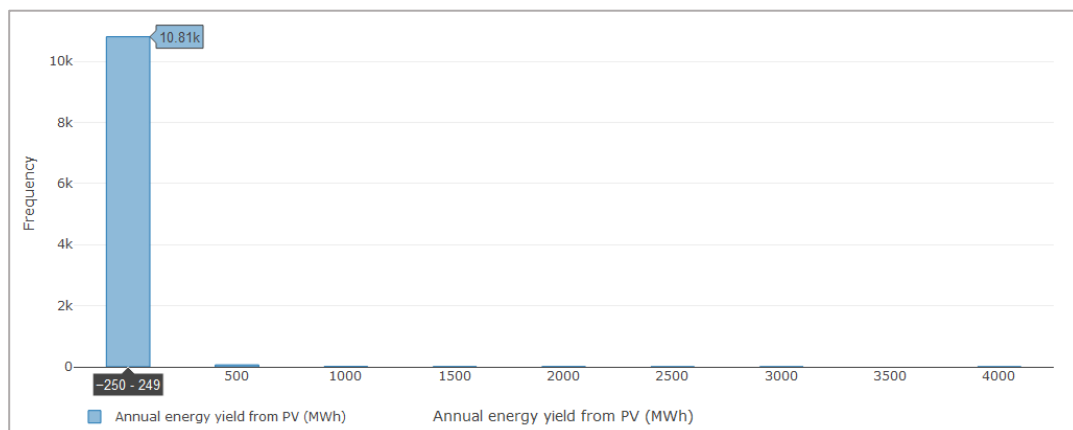
An overview map of the annual solar PV potential in Morumbi is indicated in Figure 33. A simple statistical analysis was conducted in QGIS to identify the maximum, minimum, and mean energy yield. The minimum energy yield of a single building in Morumbi is 0.96 MWh, 3839.18 MWh is the maximum, while the mean is 40.22 MWh. The total energy yield from solar PV in the whole study area is 43,8184.59 MWh.





**Figure 33 Annual solar PV potential in Morumbi**



The value distribution range between the mean value and the maximum value is quite significant. This phenomenon is caused by the uneven value distribution of solar energy yield. The produced solar energy is highly dependent on the roof surface dimension. Due to the fact that most of the buildings in Morumbi are residential buildings, the solar energy that can be generated from an individual building falls within the range of 0 to 249 MWh per year. A more explicit depiction of the data distribution is indicated in a histogram within Figure 34.



**Figure 34 Annual energy yield histogram**

Buildings that produce solar energy from 0 to 249 MWh per year reach 10,810, which is 99% of the total suitable building in the study area. The number of buildings that generate higher solar energy is relatively low, only 1% of the total suitable buildings. The property types that fall under this category are non-residential building, such as office building, shopping arcade, stadium, etc. Buildings with the largest and smallest available area for the solar PV installation d is the following:

Table 5 Buildings with the smallest and largest available area for the solar PV installation

	<b>Smallest available area for solar PV installation</b>	<b>Largest available area for solar PV installation</b>
Coordinates	23° 34' 48" S, 46° 43' 12" W	23° 35' 59" S, 46° 43' 9" W
Annual energy yield (MWh)	1.19	3,839.18
Area for PV installation (m <sup>2</sup> )	10.25	17,022.25
Preview picture (overlaid with Orthophoto from Geosampa)		

The building with the highest value of solar PV potential in Morumbi is a stadium. It is in line with the dimension of the suitable area for solar PV installation, as the available area of the stadium is also the highest among all buildings in Morumbi. Location wise, there is no building in the surrounding area that blocks the incoming solar radiation. Therefore solar radiation can be absorbed effectively by the roof surface of the stadium.

Meanwhile, the building with the smallest available area for the solar PV installation is basically surrounded by taller buildings. It can be seen from the preview picture that there is a shadow cast impacted by the building at the northern side of the premise. The available area for PV installation is very limited, close to the standard minimum area of solar PV installation. These factors influence the low annual energy yield of this building.

Other results derived from the solar PV potential modelling are the PV capacity and CO<sub>2</sub> emission savings. The total PV capacity in the Morumbi area is 20,5238.24 kWp or 205.23 MWp. The total CO<sub>2</sub> emission that can be saved is 122,691,912 kgCO<sub>2</sub>e or 122,691.91 metric tons. Referring to the data from Muntean et al. (2018), that the CO<sub>2</sub> emission per capita in Brazil is 2.3 t CO<sub>2</sub>/year, in the case of the whole feasible rooftop surface in the study area will be utilized for solar PV installation, the PV installation will offset the CO<sub>2</sub> emission within the whole year from approximately 53,343 individuals.

### **Impact of the panel inclination adjustment**

The panel inclination highly influences the amount of solar radiation received by the PV panel. This section elaborates on the impact of panel adjustment on the flat-roof surface based on seasonal change. The analysis was carried out on the flat-roof surface only because the roof's slope on the non-flat roof surface (pitched, gabled, dome) are fixed. Hence the adjustment of the panel inclination would be challenging or even nearly impossible. The analysis of the seasonal panel adjustment is indicated in Table 6.

Table 6 Seasonal-based panel adjustment

Month	Season	Inclination	Aspect	Mean daily solar radiation (Wh/m2)
March	Autumn	23°	90° (head north)	6610.26
June	Winter	25°	90° (head north)	4649.61
September	Spring	23°	90° (head north)	6235
December	Summer	No modification	90° (head north)	7952.86

In the autumn season (March), the highest amount of solar radiation was obtained by modifying the panel inclination to 23° and rotate the panel to be headed north. In June (winter), to receive the most solar radiation on the panel surface, the inclination should be tilted to 25° and rotate to the north. During September (spring), the best setting for solar panel inclination is 23° and heading north. Without modifying the panel inclination but rotating the panel to the north in December (summer), the PV panel will perform better. It should be noted that this analysis would not be incorporated with the real-sky solar radiation layer displayed in the visualization.

### Validation

In order to predict the model accuracy, error estimations for the solar radiation and energy values had been calculated. The method for calculating the error of the model was by calculating the Mean Absolute Error (MAE) and Mean Absolute Percentage Error (MAPE). These methods were selected since they will perform better in measuring the average error rather than other methods such as Mean Square Error (MSE) and Root Mean Square Error (RMSE). MSE and RMSE are ambiguous and adding more weight to the extreme value, hence they are inappropriate and misinterpreted measure of average error (Willmott & Matsuura, 2005). MAE is calculated by averaging all residuals from each data point. MAPE is the percentage of MAE. It is the ratio of the residual over the actual.

For calculating MAE and MAPE of solar radiation data, the predicted daily average values from each month were compared with three solar radiation datasets. First, data from Ourinhos meteorological station (22 ° 56' 55" S, 49 ° 53' 39" W), a meteorological station maintained by SONDA, "Sistema de Organização Nacional de Dados Ambientais" [National Environmental Data Organization System], a project by the National Institute for Space Research (INPE) Brazil (INPE, 2019). Another solar radiation data from LABREN Brazil (Laboratory for Modeling and Studies of Renewable Energy Resources Brazil) derived from BRASIL-SR radiative transfer model, with the input parameter from 17 years of satellite data (Pereira et al., 2017) were used in the validation process. Lastly, the validation used monthly mean average solar radiation from ERA5 reanalysis data produced by the Copernicus Climate Change Service (C3S) at the European Centre for Medium-Range Weather Forecasts (ECMWF) (ECMWF, 2021). The error calculation is based on the daily average solar radiation for each month. Table 7 indicates the sample values, and Figure 35 shows the better visualization of the comparison.

Table 7 Data for the error prediction

Month	Mean daily solar radiation from the model (Wh/m <sup>2</sup> )	Mean daily solar radiation from the SONDA (Wh/m <sup>2</sup> )	Mean daily solar radiation from LABREN (Wh/m <sup>2</sup> )	Mean daily solar radiation from ERA5 (Wh/m <sup>2</sup> )
January	5,238.64	5,462.56	5,251.00	6542.11
February	5,336.63	5,256.46	5,428.00	5273.68
March	4,615.86	5,617.24	4,636.00	4950.6
April	4,186.93	4,796.62	4,138.00	4379.57
May	3,386.23	4,064.79	3,358.00	3554.17
June	3,069.07	3,129.85	3,091.00	3629.09
July	3,284.33	4,095.94	3,201.00	3831.16
August	4,026.13	4,048.84	4,070.00	3960.06
September	3,813.13	5,164.28	4,093.00	4677.85
October	4,613.88	4,326.75	4,545.00	5935.98
November	5,161.03	5,557.71	5,101.00	5278.69
December	5,698.35	6,706.02	5,636.00	5686.81

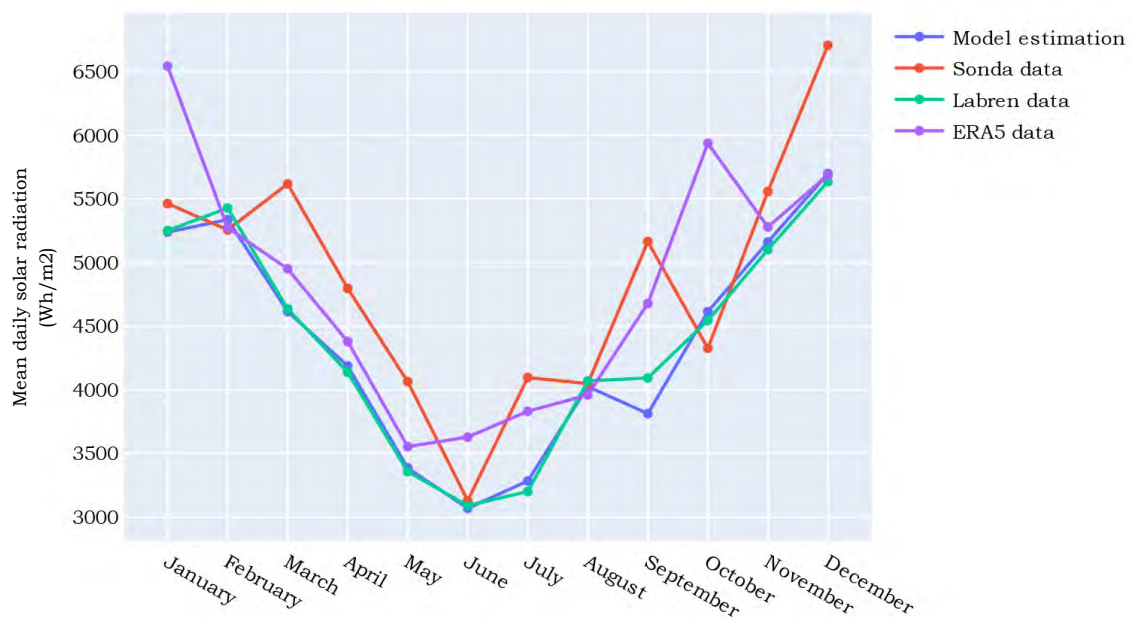


**Figure 35 Comparison between estimated data from the model with control data**

From the chart, it can be identified that data from the model and LABREN data shows a similar trend. However, when the model data is compared with SONDA data, there are some trend anomalies. For instance, in the model data, the daily mean solar radiation value in September is lower than in October, wherein the SONDA data value in September is higher than in October. The most significant discrepancy is indicated by the comparison with ERA5 data, as solar radiation values are higher than the predicted values.

The MAE and MAPE of the data were calculated in Python using the *scikit.learn* library. The result is indicated in Table 8.

Table 8 MAE and MAPE assessment

	<b>Model prediction vs SONDA data</b>	<b>Model prediction vs LABREN data</b>	<b>Model prediction vs ERA5 data</b>
MAE	544.28	68.44	1393.58
MAPE	10%	1.6%	21.85%

The data obtained from the model with empirical data from LABREN shows a lower average error than data from SONDA and ERA5. It is possibly due to the fact that LABREN data also resulted from a model calculation, thereby, it gave closer values with the model prediction in Morumbi. In contrast, SONDA data are obtained from in-situ measurements. The discrepancy from the comparison with ERA5 is the largest, proofed by both MAE and MAPE values. Several publications have mentioned that ERA5 data produce large bias under cloudy or overcast condition. Overestimating under cloudy conditions suggests inaccurate prediction of cloud patterns and leads to larger absolute errors (Urraca et al., 2018). Solar radiation values from the ERA5 dataset also tend to be overestimated compared to data from ground observation (Sianturi et al., 2020). Considering that, the error value from ERA5 was not taken into account in this work.

Lewis (1982) suggested four categories to interpret MAPE values for evaluating a forecasting or prediction model, indicated in Table 9. Thus, disregarding the error assessment of ERA5 data, the solar radiation modelling based on *r.sun* in this thesis can be concluded as a reliable model as it falls between good and highly accurate prediction model according to Lewis (1982) interpretation.

Table 9 Typical MAPE values interpretation (Lewis, 1982)

<b>MAPE value (%)</b>	<b>Interpretation</b>
<10	Highly accurate prediction
10-20	Good prediction
20-50	Reasonable prediction
>50	Inaccurate prediction

In regards to the annual solar energy, fifteen buildings were selected to be used as the data sample using the stratified sampling method. The list of building samples and their values can be seen in Table 10. Sample one to five corresponds to large buildings (greater than 275 m<sup>2</sup>), sample six to ten consists of medium-size buildings (100 to 275 m<sup>2</sup>), and sample 11 to 15 area small size buildings (less than 100 m<sup>2</sup>). Because there is no valid solar energy data available in the study area or nearby locations (equal latitude) with similar area size, the model was compared with the output from the PV Watts calculator, a tool created by NREL for estimating the performance of PV installations (NREL, 2021).

Table 10 Building samples and their annual solar energy values

No. of sample	ObjectId	Annual solar energy predicted by the model (MWh)	Annual solar energy from PV Watts (MWh)	Available area for PV installation (m <sup>2</sup> )	Roof shape (flat/non-flat)
1	429	202.7	214.6	1689.19	flat
2	471	164.77	175.38	1117.25	non-flat
3	500	46.52	50.08	72.75	non-flat
4	9105	127.07	126.76	538	non-flat
5	2194	75.74	78.48	354	flat
6	9169	40.13	35.1	168.25	non-flat
7	7389	64.91	62.2	113.75	non-flat
8	10314	47.81	41.62	187.75	flat
9	2673	50.22	47.46	200.75	flat
10	1701	39.08	37.91	171	flat
11	3637	16.79	15.24	68	flat
12	3857	17.14	16.99	72.75	non-flat
13	1650	9.84	10.46	47.25	flat
14	197	14.69	14.23	64.25	non-flat
15	1790	6.43	7.02	30	non-flat

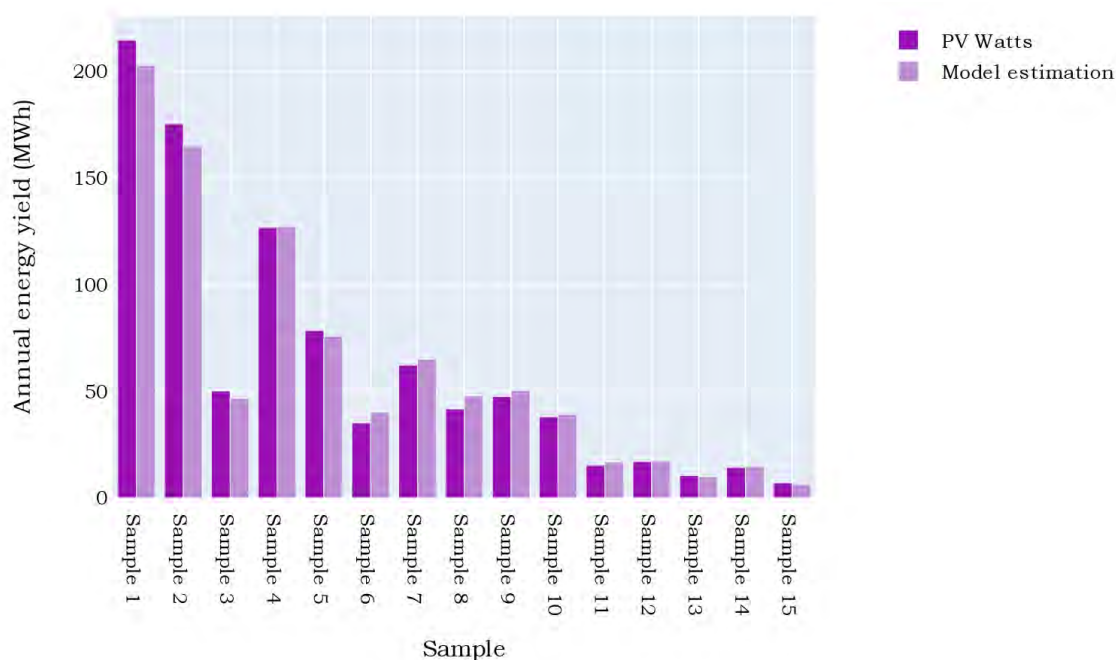


**Figure 36 Comparison of solar energy values from the model vs PV Watts**

According to Figure 36, the estimation from the model tends to be lower than the output from PV Watts for large-size buildings. The most significant discrepancies are also indicated on samples correspond to large scale buildings, i.e. sample 1 and 2. On the



other hand, the model prediction on medium-scale buildings consistently shows higher values than PV Watts's output. Minor differences are indicated on small-size building samples. In summary, the larger the surface area, the higher chance of discrepancy occurs between PV Watts's output and the model prediction.

The result of MAE and MAPE can be seen in Table 9. It shows that the average absolute error is 3.35, while the mean absolute percentage error is 6%. Also, referring to Lewis (1982) interpretation in Table 9, the model can provide a highly accurate prediction of solar PV potential in Morumbi.

Table 11 Error assessment of the model prediction vs PV Watts

	Model prediction vs PV Watts
MAE	3.35
MAPE	6%

## 6.2 Visualization of results

The output of the visualization represents in digital formats by a web-map application and 3D CityGML. Through such media, possible targeted users, i.e. the government, citizens, energy planners and solar engineers, could explore the solar PV potential in their area.

### Web-map application

The web-map application was built based on the OpenLayers library. It displays the information in an interactive map of the solar radiation layer, annual solar energy generated from PV, and unsuitable building for the PV installation. The map is complemented with basic features such as pan, zoom in-out, etc. and additional functionalities for better interactivity on the client-side. The interface of the web-map application and its functionalities are indicated in Figure 37. The stable version of the web-map application is hosted within Apache Tomcat Server at the Department of Geoinformatics, Palacky University Olomouc. It can be accessed through this link: [http://158.194.94.29:8081/webgis/solar\\_map\\_morumbi.html](http://158.194.94.29:8081/webgis/solar_map_morumbi.html).

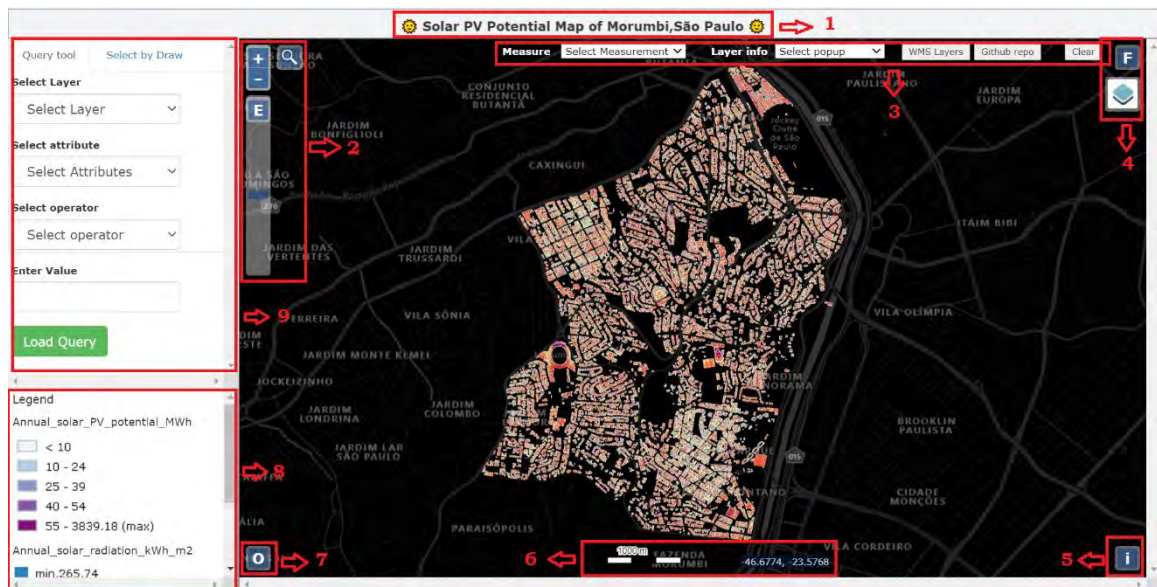


Figure 37 Web-map application interface including the functionalities

The description of each web-map application functionality is the following:

## 1. Map heading

The heading part shows the title of the map. The title is tagged as `<marquee>` HTML element, which adds a scrolling effect to static text.

## 2. Toggle zoom in-out, zoom extent and geocoding control

Users will be able to control the extent of the map view using the zoom in and out toggle buttons. The web-map application also includes zoom extent and slider control. The zoom extent function (letter E button) allows users to change the map view to the default zoom level. The zoom slider control provides a similar function as the zoom in-out button but with a smaller zoom level interval. The button with the magnifying glass symbol is the geocoding control. It has the ability to search a particular address, venues or coordinates from an input by the user. The geocoding feature is based on OpenStreetMap Nominatim API, an open-source geocoding API service provided by OpenStreetMap. Figure 38 shows the example of the geocoding application. In this example, the user is searching for Morumbi stadium or *Estadio Morumbi*. After pressing enter, the map display will zoom in to the stadium coordinate.

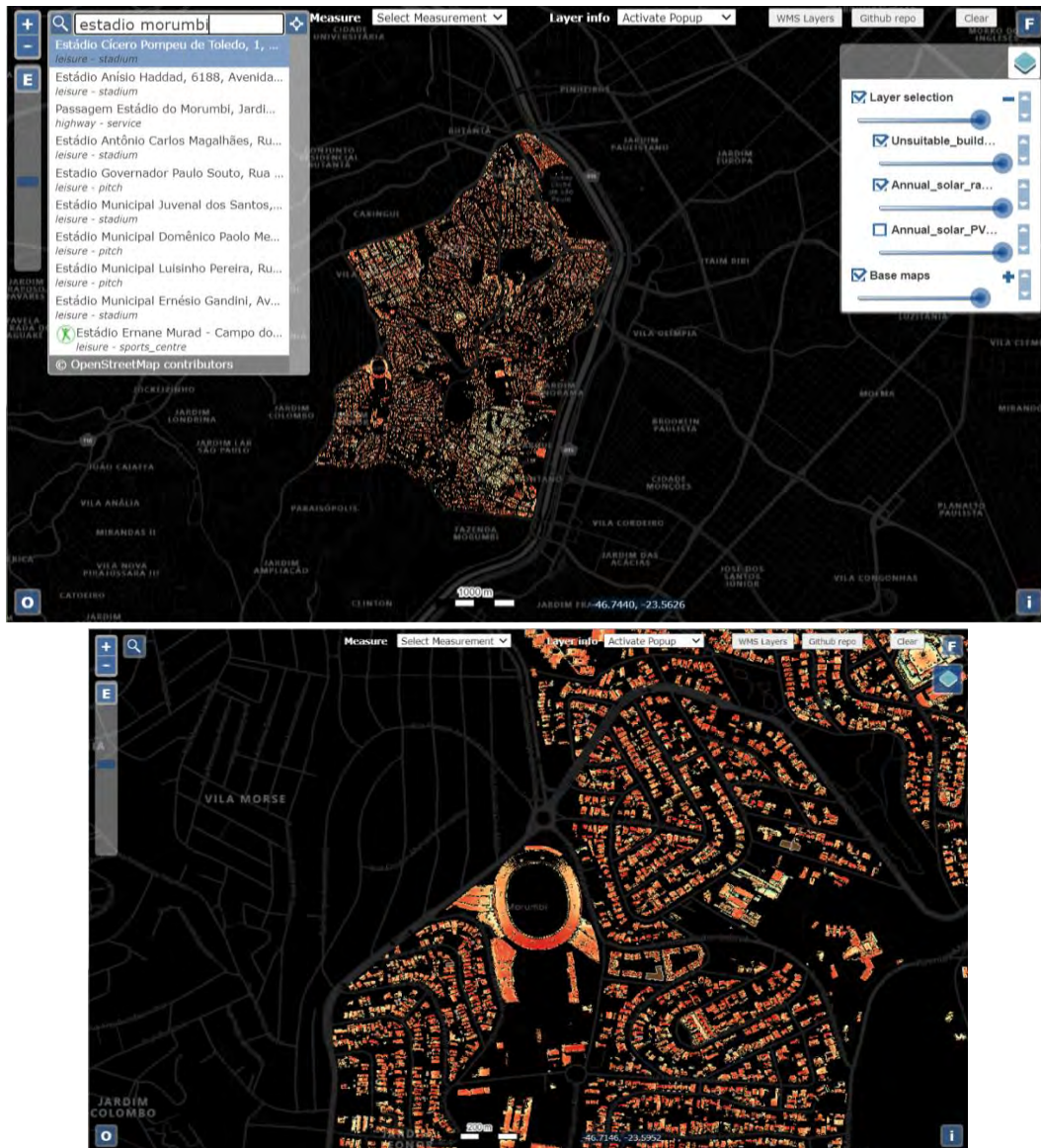


Figure 38 Application of the geocoding control



### 3. Advanced functionalities

These functionalities offer more advanced control by the user. It includes measurement tools, pop-up control, additional WMS layers, a link to the Github repository, and a Clear all button.

#### a) Measurement tools

The user can use the tool to measure distance (unit in km) and area (unit in km<sup>2</sup>). The measurement will automatically appear on the screen when the user draws the line or the area.



Figure 39 Example of the area measurement tool

#### b) Pop-up control

A pop-up function displays the attribute associated with each feature layer (Esri, 2021). In this case, the pop-up attributes are derived from the WMS feature info of each layer. It means that if the pop-up function is activated, each time the user clicks on a feature, the server will be communicating with Geoserver to derive the feature info using *GetFeatureInfo* request. The feature info is then displayed as feature attributes within the pop-up dialogue box.

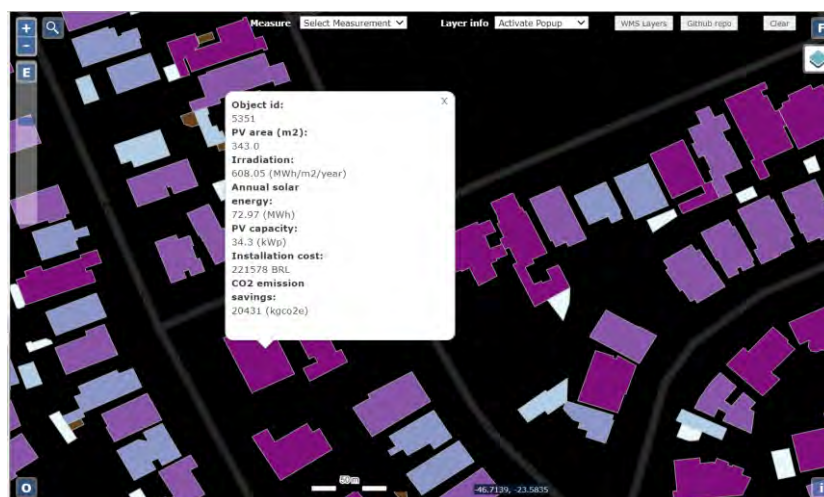


Figure 40 Pop-up display

#### c) WMS layers

Since only three layers are displayed on the default interface, the WMS layers function allows the user to add additional WMS layers that have been published on Geoserver.



**Figure 41 Additional WMS layers window**

#### **d) Github repo button**

This function allows the user to explore the GitHub repository of the web-map application project. The Github repository also plays the role of a connector in the spatial data infrastructure between the visualization interface, in this case, is the web-map application and the distribution platform of data. Within the GitHub repository, the user can look into the application source code, download layers as KML, download the CityGML model and inspect the metadata. There is also a link to download layers via Google drive.

#### **e) Clear button**

The clear button allows the user to reset the view to default. All selections and measurement drawings would be removed from the map view.

### **4. Toggle fullscreen and layer selection control**

The fullscreen button enables the fullscreen mode. The user is able to switch back to windows mode simply by pressing the *Esc* button on the keyboard. The layer selection control enables the user to switch on and off available layers and change their transparency by moving the slider below the layer title. Within the layer selection tab there is also a feature for selecting the basemap.

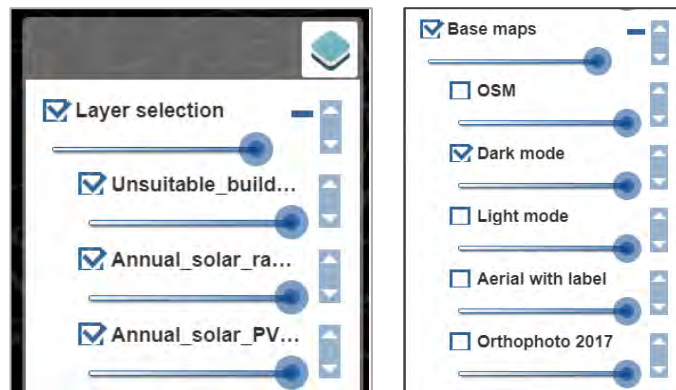
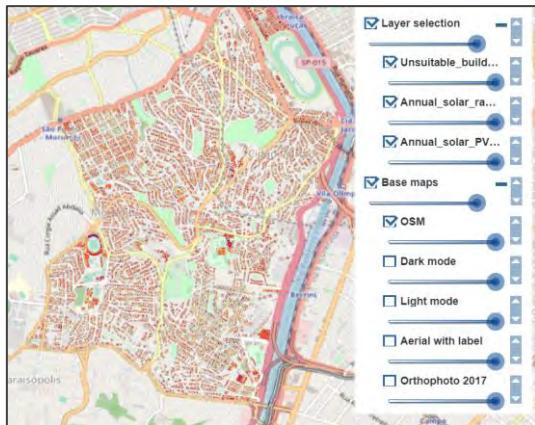


**Figure 42 Layer selection tab**

The web-map application is complemented with five switchable basemaps. Users will be able to select the base map according to their preference. *OSM* basemap is a tile server provided by OpenStreetMap. *Dark mode* and *Light mode* were derived from TomTom datasets which are served by BingMaps and accessible via their API request. The default basemap selection is *Dark mode*. *Aerial with label* is also based on BingMaps which displays aerial imagery and place labels. The last available basemap selection is *Orthophoto 2017* which displays the orthophoto tile server from Geosampa. This tile server is accessible using WMTS *get* request. However, it should be kept in mind that the rendering speed highly depends on the load of the Geosampa server.





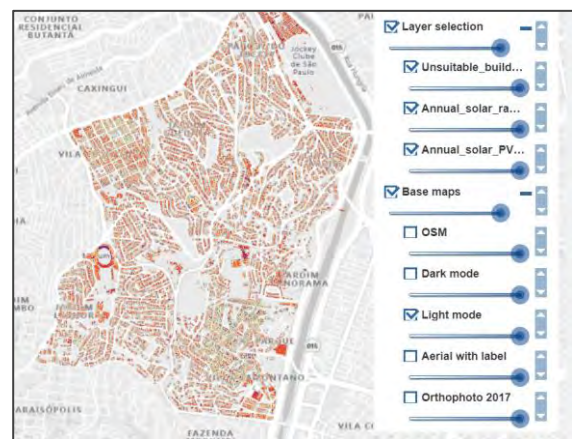
(a) OSM basemap



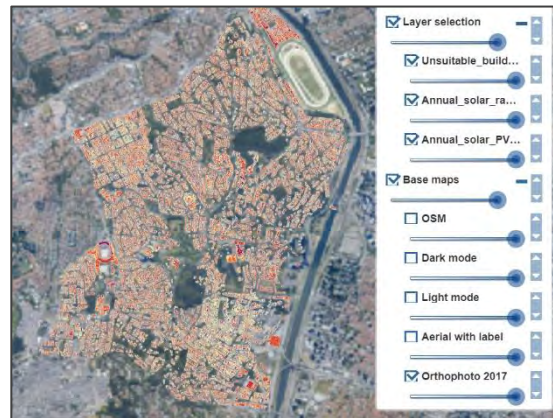
(b) Dark mode basemap



(c) Light mode basemap



(d) Aerial with label basemap



(e) Orthophoto 2017 basemap

**Figure 43 Available basemaps on the web-map application**

## 5. Attribution

By clicking the *i* button, the attribution information, including copyrights and licences, will be displayed.

## 6. Scale bar and mouse position

The scale bar displays the scale of the map view in meter. The mouse position function displays the coordinate (in decimal degrees) of the current mouse position.

## 7. Overview map

The overview map button allows the user to display the overview map based on the OpenStreetMap base map tile layer.

## 8. Legend box

Generally, the OpenLayers library does not offer legend functionality. Therefore, the legend is displayed in the web map by executing a `getLegendGraphic` request in Geoserver via a JavaScript function. The `get` request for displaying the legend is the following:

```
http://158.194.94.29:8081/geoserver/solar_pot/ows?service=WMS&request=GetLegendGraphic&format=image%2Fpng&WIDTH=15&HEIGHT=10&legend_options=fontName:Verdana;fontSize:5;fontAntiAliasing:false;dy:0.2;dpi:200;wrap:true&layer="+overlays.getLayers().item(i).get('title')
```

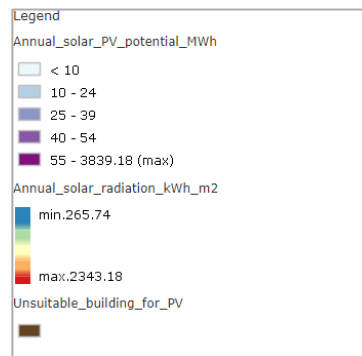
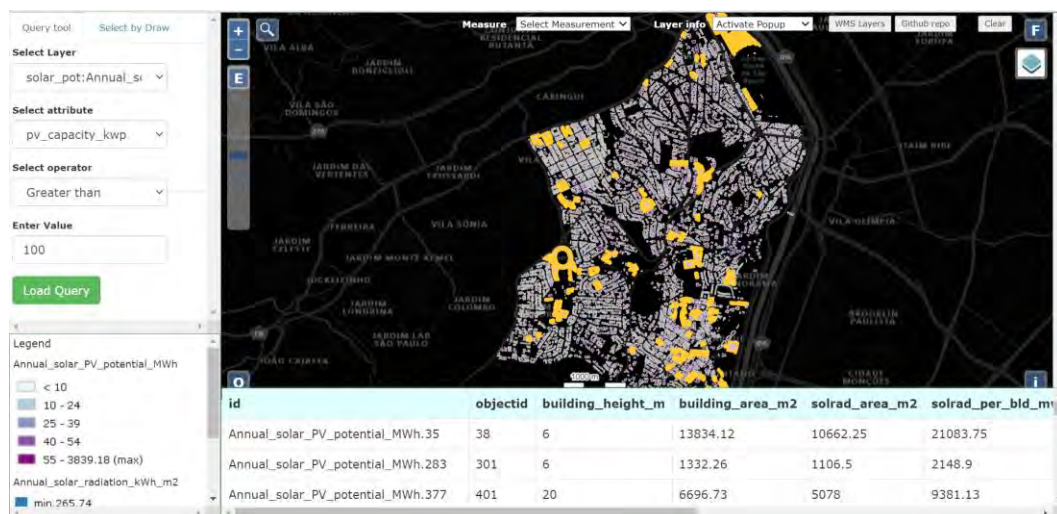


Figure 44 Legend box

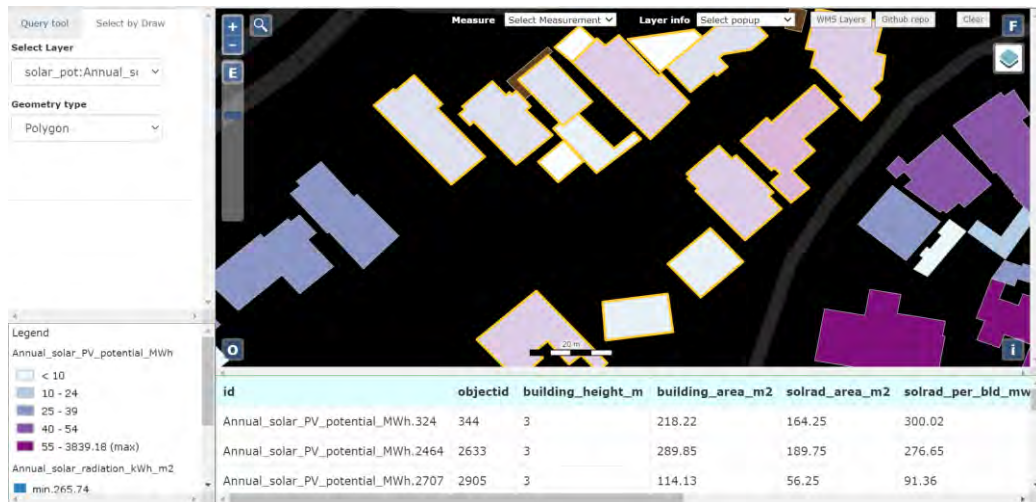
## 9. Query functions

Query functions are widely used in GIS, especially for select a subset of the layer attribute based on specific criteria declared by the user. The solar PV potential map also offers such functionalities. There are two query options available. The *query tool* enables the user to select the feature based on attributes. The tool includes a comparison operator (less than, greater than, and equal to) under the *select operator* menu. Another available query option is *Select by Draw*, which allows the user to select features by drawing a geometric shape.



(a) Query tool interface





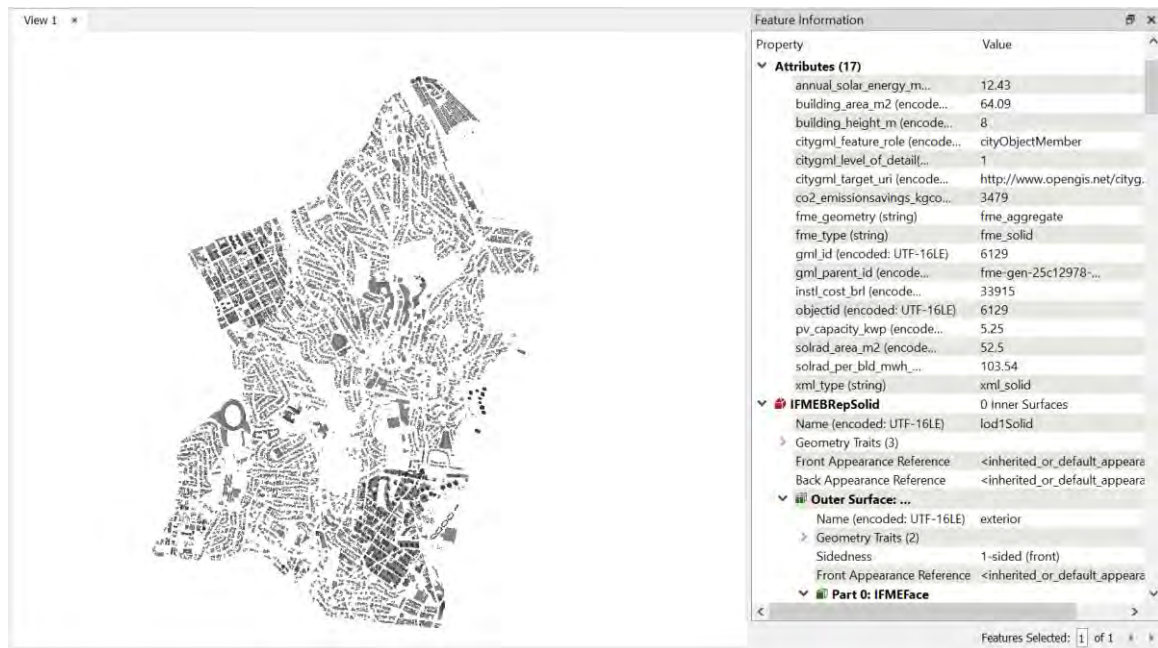
(b) *Select by Draw* interface

**Figure 45 Query functions**

### CityGML result

As previously described in Chapter 5.4, the CityGML file stores all model attributes in an XML-based document. It also contains information about the model's level of detail and the GML ID. The level of detail of the generated model is Level 1 Solid (LoD1Solid). The CityGML document can be opened using compatible software, such as FME Safe Software, Bentley Map or VC Suite.

It should be noted that the feature inspector in FME Safe Software cannot visualize 3D models in the EPSG:4326 coordinate system. The model needs to be reprojected to a projected coordinate system. Therefore, the output of the CityGML model is in EPSG:31983, which is the original coordinate system derived from the original building footprint layer (SIRGAS 2000 / UTM Zone 23S). Figure 46 represents the model view when opened on FME Safe Software.



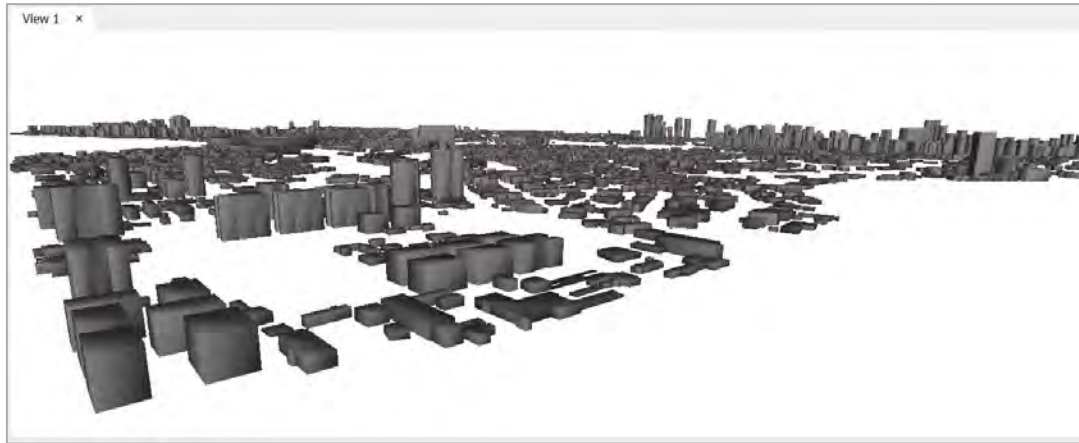


**Figure 46 CityGML model view on FME Safe Software**

As can be seen from the visualization, the CityGML document's output is able to convey the information of solar potential in Morumbi and display it in 3D. Unlike the 2D raster and vector approaches, the 3D visualization brings closer depiction to reality. The current LoD1 Solid city model can also be further enhanced by increasing the level of detail, which will leverage the visual aspect of the model.

## 7 DISCUSSION

As the obtained result has been elaborated in Chapter 6, some points need to be highlighted in more detail. This chapter amplifies the prospect of applying the output beyond the extent of this thesis. Moreover, issues that arose during the work process are mentioned within this chapter.

### 7.1 Data suitability

The availability of open data source in the study area simplifies the data acquisition process in this thesis. The primary input of the model is the topographical data which was easily derived from the Geosampa web portal. The point cloud data is in a very high resolution and already classified. Hence, it did not require too much pre-processing work before it used for the later stage of the modelling workflow.

On the contrary, the process of acquiring the atmospheric parameter was more complicated. For obtaining accurate solar radiation values from the model, detailed climate or atmospheric attenuation datasets are required. Ideally, the interval or temporal resolution of the atmospheric attenuation data should correspond to the time step parameter that has been set before running the model. In this case, the time step selected was 0.5 hour (30 minutes). However, there is no atmospheric dataset with 30 minutes temporal resolution available. The SoDA website only covers monthly aggregation of Linke turbidity value, which is based on the fusion of gridded data from NASA, precipitable water vapour (NVAP), aerosol optical depth (pathfinder) and ground information about turbidity from radiation or aerosol measurements (AERONET) datasets (MINES ParisTech / Transvalor, 2021). The lower temporal resolution of atmospheric attenuation parameters definitely affects the level of accuracy of the model output. Therefore, anomalies were detected during the error assessment, especially when compared with ground station data. It is expected that the atmospheric attenuation dataset with a higher temporal resolution will be available in the future to be able to be used for more advanced and accurate solar radiation modelling.

The building footprint dataset only represents the roof area, and it does not include the roof surface classification, which signifies that the shape of the roof (gabled, pitched, dome, etc.) could not be identified from the current dataset. Indeed, the roof surface classification can be conducted using image classification or machine learning techniques. However, the process of conducting the abovementioned technique will be taking up most of the time allocated for the analysis, and it is beyond the scope of this thesis. As a result, the building suitability layer contains the information on the available area for PV installation is visualized by a single polygon feature rather than depicting the available area of each roof surface.

There are two meteorological stations relatively close to the study area, IFUSP and IAG USP stations. However, the IFUSP meteorological station only records irradiance data from a pyranometer from 2004 to 2018. Within a quite significant period, especially in 2018, the instrument was under maintenance. Thus, the irradiance value was unrecorded. Since IAG USP data were used for computing clear-sky index ( $K_c$ ), there was a lack of data on irradiation or irradiance available for validation. If more irradiation data is available in the study area or surroundings, there will be more control data for validation, which increases the degree of confidence of the model. The  $K_c$  values would also be more accurately estimated by performing spatial interpolation of the  $K_c$  value, acquired by calculating the ratio of GHI from multiple ground stations over the GHI during a clear-sky condition at the ground station location.

## 7.2 The modelling process

Solar radiation is the most crucial component with regards to the estimation of solar PV potential. Either by obtaining the value from an in-situ measurement, satellite data or modelling, solar radiation parameters must be as accurate as possible. The algorithm based on the *r.sun* module in GRASS GIS is quite reliable for calculating solar radiation. It is indicated in the validation section in this thesis that although some anomalies were present when the prediction is compared with ground station data, the absolute error is relatively low when the prediction was validated against the LABREN model. Arguably, from the performance point of view, the solar radiation computation based on the *r.sun* module is in the same level of accuracy as a model that uses multiyear satellite data as the input.

With regards to the solar PV potential modelling, the result was pretty much determined by the quality of input parameters. The variety of geographical characteristics, even at the building scale, greatly influences the output of the PV installation on each building. The main finding of this study is that GIS can be considered an efficient methodology to model the potential of solar PV in the urban area. It is proven by the result of this thesis that there is plenty of valuable information can be delivered to the stakeholders and decision-makers using GIS during the initiation phase of solar PV development in the urban area. The information could be the PV capacity, installation cost, CO<sub>2</sub> emission savings and many more.

Further assessment of the study area's modelling result shows that the solar PV potential in the study area is abundant. The fact that the study area lies relatively close to the equator brings an advantage since the region receives more proportion of direct sunlight. By conducting the panel inclination analysis, it could be identified that the seasonal change of the sun position is one of the aspects that highly weighs the amount of energy yield on a surface. However, it must be kept in mind that the approach for assessing the impact of panel inclination adjustment in this study is experimental and requires more comprehensive analysis.

As previously stated in section 6.1, 92% of buildings in Morumbi are feasible for solar PV installation. However, it must be noted that in reality, there is a high possibility this percentage is decreasing. Many factors have to be taken into account in designing a PV system that directly or indirectly influences the building feasibility. For instance, the operation cost will be higher for a building with a complex roof structure, which affects the length of the payback or breakeven point period. Thus, even though the area is viable for solar PV installation, it might be not the case from an economic point of view. Such research about the solar PV potential assessment should ideally be supported with sensitivity analysis.

Concerning the complexity, it is evident that there was much interfacing effort during the modelling process. Six different software were utilized for the modelling process, with most of it consumed a large portion of the computer RAM. The multitasking task was hard to execute since the amount of memory usage exceeded the maximum capacity. This problem can be overcome by creating a script (e.g. via Python, R or Shell) that will automatically execute inter- or intra-software tasks. One example of the scripting application was carried out in this thesis via Python during the iteration of the *r.sun* module to obtain the annual solar radiation. Furthermore, for future studies, an end-to-end script is worthwhile since it will increase the reproducibility of the research.

### 7.3 Visualization process

The biggest challenge in the visualization part was the preparation of the back-end environment of the web-map application. The unavailability of a dedicated server for installing Geoserver prompted the author to establish a local server based on Apache Tomcat to install Geoserver and publish the web-map application. Consequently, the web-map application can only be accessed by exposing the IP address, which raises the security concern. The aforementioned problem also hinders the opportunity to share the web-map application and perform user testing to possible targeted users. Hence, when producing similar research, it should be ascertained that the back-end environment is well established and compatible with the intended use component for extending the interoperability. One alternative is to use a Virtual Private Server (VPS) for running Geoserver instances. Another solution is to utilize cloud-based mapping services such as ArcGIS Online or Mapbox, however, functionalities offered by cloud solutions are limited.

The author chose OpenLayers as the map library for the front-end framework. The main reason is that OpenLayers offers many functionalities and APIs related to GIS applications, and it is fully open-source. OpenLayers can also read OGC-standard web services such as WMS and WFS without adding plugins as this feature is already integrated within its API. However, despite its powerful performance and flexibility, there was a learning curve in the code deployment. Functions in OpenLayers require more JavaScript code than other map libraries such as Leaflet or GoogleMaps API. The total length of code for the whole web-map application, including HTML syntaxes and comments, is 2082, a quite extensive length of code for a single page web map application.

The availability of 3D point cloud data provided the author with an idea to visualize buildings in the study area in 3D and store them in CityGML format. It allows the 3D model to store attributes, in this case, is solar PV potential attributes (same attributes as the annual solar PV potential vector layer). Unfortunately, the building footprint layer from the Geosampa web portal is only represented by simple 2D polygons. Currently, there is no available data on the 3D building model available in the study area that provides the information of the roof surface. Thus, the maximum outcome that could be achieved in this thesis is a LoD1 city model. In the early formulation stage of this thesis, the author intended to publish the 3D building model into a web-map application through the Cesium platform. However, during the process, the author encountered a problem with the coordinate system since Cesium only supports the EPSG:3857 (Web Mercator) coordinate system. After reprojecting from EPSG:31983 to EPSG:3857, the model was not appropriately placed on where it is supposed to be located. As there is a possibility that it is a bug of Cesium itself, the author has sent a new thread to the Cesium discussion forum. However, there was no response from the forum member that leads to a solution to this problem.

All in all, it can be deemed that a web-map application is an efficient way to visualize such analyses. With its interactivity, much valuable information can be accessed from anywhere and anytime to prospective users to support the design phase of solar PV installation in the urban area.

### 7.4 Future perspective

GIS-based Solar PV potential modelling is not trivial, especially for increasing renewable energy generation in the urban area. Future research on this topic should be supported with credible datasets and consider more factors such as roof material and shadow aspect, to improve the modelling result. The inclusion of machine learning and

image recognition techniques will definitely provide added value to the research, for instance, in classifying the building's roof surface. Moreover, for a better user experience in the solar PV potential assessment at the building scale, developing a GIS-based tool that offers more customization, e.g. the ability to change the model input parameter (e.g. panel inclination, drawing the roof area, orientation) on the go, complemented with API service, will be a subject of future work.

In addition, adding building categories (e.g. public facilities, government office, small-scale residential, large scale residential) will provide a more informative solar PV potential assessment. Such information is advantageous for tracking the correlation between the purpose of the building, electricity usage, and the productibility of the PV system.

Furthermore, calculating solar PV potential on building facades has to be accounted for to maximize the extent of the research. Since recently, solar panels are not only able to be mounted on a roof surface but also on the building façade. The study in the future also needs to consider the visualization using a LoD3 MultiSurface CityGML model. It is recommended to colour-code the building model based on the solar PV potential attribute, for instance, the annual energy yield. A project funded by the European Union, i-SCOPE, which focuses on smart city development, can be a good reference for future studies. The project develops a CityGML model that includes Application Domain Extension (ADE) on solar energy potential assessment and noise level on the urban scale (I-SCOPE, 2021).



## 8 CONCLUSION

The main goal of this thesis was to utilize the GIS approach to model the potential of solar rooftop PV in the urban area, which will support the initial process in designing a proper solar photovoltaic system. There were objectives to be fulfilled to achieve the goal of the thesis. The first objective was to identify a GIS-based algorithm to model the solar PV potential. It included the literature review and extensive research on the available algorithms. According to the literature, some algorithms are widely used in estimating solar PV potential. One of them is the *r.sun* module. The *r.sun* module was finally selected as the algorithm for the modelling process.

The study area focuses on the Morumbi district, São Paulo, Brazil. All datasets that used in this thesis were entirely derived from open-data sources. The first stage of the modelling process was to generate a DSM from point cloud data, then calculate solar radiation of the surface. The solar radiation is based on the *r.sun* module that incorporates topographic and atmospheric parameters in its algorithm. It proved to effectively address the complicity in identifying solar energy potential from photovoltaic installation in the study area, specifically at the building level. Unlike conducting an in-situ measurement, this model is more cost-efficient as it could cover a much larger area for prediction. Finally, the result is visualized within an integrated spatial data infrastructure. It facilitates the discovery and access of data through downloadable layers in KML and GML as well as web services such as WMS and WFS.

The result provides an insight that by running a GIS-based model, the abundance of the solar PV potential in Morumbi could be identified. In regards to solar intensity, the comparison of daily average solar radiation in Morumbi with the solar radiation value from other regions in the world with equivalent latitude could be identified. Through the result, the monthly average trends of solar radiation could also be identified. The percentage of suitable buildings for the solar PV installation is high, reaches 92% of the whole building in the study area. Additional analyses on calculating PV capacity, installation cost, CO<sub>2</sub> emission savings, and the panel inclination impact assessment were also carried out. The finding obtained from the assessment on the impact of the panel inclination adjustment was that seasonal trends of the sun position and topographical features such as aspect and slope highly determined the amount of solar radiation received by the surface. The result also indicates the strong potential of solar energy in the area, which will be contributing to the city's sustainability if the energy is being exploited.

It can be concluded that the aim and objectives of this thesis were accomplished. The result of the model could provide the information that the GIS-based algorithm is robust for determining solar radiation in the study area. The entire modelling workflow can also be applied to solve a similar task in other study areas. Nonetheless, there are still places for further enhancement in this study. To increase the prediction accuracy, the comprehensiveness of input datasets obviously determines the quality of the model output. More advanced visualization and putting more effort into the interoperability aspect of the spatial data infrastructure should also be considered to ensure the information is well-perceived by the targeted user.

## REFERENCE AND INFORMATION SOURCES

- AGUGIARO, G., NEX, F., REMONDINO, F., FILLIPI, R., DROGHETTI, S., & FURLANELLO, C. (2012). Solar Radiation Estimation on Building Roofs and Web-Based Solar Cadastre. *ISPRS Annals of the Photogrammetry, Remote Sensing and Spatial Information Sciences*, I(2), pp. 177-182. doi:10.5194/isprsannals-I-2-177-2012
- AKTARUZZAMAN, M., SCHMITT, T. (2011). Detailed Digital Surface Model (DSM) Generation and Automatic Object Detection to Facilitate Modelling of Urban Flooding. *ISPRS Archives*, XXXVIII(1), p. 7.
- AMADO, M., POGGI, F. (2014). Solar Energy Integration in Urban Planning: GUUD Model. *Energy Procedia*, 50, pp. 277-284. doi: 10.1016/j.egypro.2014.06.034.
- ArcGIS Online Help: Configure pop-ups*. 2021 [cit. 2021-05-05]. Esri. Available online: <https://doc.arcgis.com/en/arcgis-online/reference/configure-pop-ups.htm>
- BAFGHI, Z., TIAN, J., ANGELO, P., REINARTZ, P. (2016). A new algorithm for void filling in a DSM from stereo satellite images in urban areas. *ISPRS Annals of the Photogrammetry, Remote Sensing and Spatial Information Sciences*, III(1), pp. 55-61. doi: 10.5194/isprs-annals-III-1-55-2016
- BLATCHFORD, M., MANNAERTS, C., ZENG, Y. (2021). Determining representative sample size for validation of continuous, large continental remote sensing data. *International Journal of Applied Earth Observation and Geoinformation*, 94(102235). doi:10.1016/j.jag.2020.102235
- Brazil - Countries & Regions - IEA*. 2021 [cit. 2021-04-18]. IEA. Available online: <https://www.iea.org/countries/brazil>
- CONTRERAS, J., SICKERT, S., DENZLER, J. (2020). Region-based Edge Convolutions with Geometric Attributes for the Semantic Segmentation of large-scale 3D Point Clouds. *IEEE Journal of Selected Topics in Applied Earth Observations and Remote Sensing*, 13(1), pp. 2598 - 2609. doi:10.1109/JSTARS.2020.2998037
- DIY Calculation Guide for 1 kW Solar System*. 2019 [cit. 2021-04-16]. Homescape. Available online: <https://homescape.solar/diy-calculation-guide-for-1kw-solar-system/>
- DUBAYAH, R., RICH, P. (1995). Topographic solar radiation models for GIS. *International Journal of Geographical Information Systems*, 9(4), pp. 405-419. doi:10.1080/02693799508902046
- ECMWF Reanalysis v5 (ERA5)* [online]. 2021 [cit. 2021-05-09]. ECMWF. Available online: <https://www.ecmwf.int/en/forecasts/dataset/ecmwf-reanalysis-v5>
- ESMAP. (2020). *Global Photovoltaic Power Potential by Country*. Washington, DC: World Bank.
- Green Power Equivalency Calculator - Calculations and References*. 2021 [cit. 2021-04-18]. EPA. Available online: <https://www.epa.gov/greenpower/green-power-equivalency-calculator-calculations-and-references>
- FERREIRA, M., OLIVEIRA, A., SOARES, J., CODATO, G., BÁRBARO, E., ESCOBEDO, J. (2011). Radiation balance at the surface in the city of São Paulo, Brazil: Diurnal and seasonal variations. *Theoretical and Applied Climatology*, 107(1), pp. 229-246. doi:10.1007/s00704-011-0480-2

*Flat roofs and balconies: Chapter 7.1* [online]. 2020-2021 [cit. 2021-05-01]. NHBC. Available online: <https://nhbc-standards.co.uk/downloads/NHBC-Standards-2020-7.pdf>

*FME — The Simple Solution for Complex Integration* [online]. 2021 [cit. 2021-05-13]. FME. Available online: <https://www.safe.com/>

*GetFeatureInfo Templates*. 2021 [cit. 2021-05-11]. Geoserver. Available online: <https://docs.geoserver.org/latest/en/user/tutorials/GetFeatureInfo/index.html>

HAILU, G., FUNG, A. (2019). Optimum Tilt Angle and Orientation of Photovoltaic Thermal System for Application in Greater Toronto Area, Canada. *Sustainability*, 11(22), pp. 1-21, doi: 10.3390/su11226443

HAWKER, L., BATES, P., NEAL, J., ROUGIER, J. (2018). Perspectives on Digital Elevation Model (DEM) Simulation for Flood Modeling in the Absence of a High-Accuracy Open Access Global DEM. *Front. Earth Sci.*, 6, p.223, doi: 10.3389/feart.2018.00233

HOFIERKA, J., SURI, M. (2002): The solar radiation model for Open source GIS: implementation and applications. *Open source GIS - GRASS users conference 2002*. Trento, Italy.

HOFIERKA, J., SURI, M., HULD, T. *r.sun* [online]. 2007-2021 [cit. 2021-05-11]. GRASS 7.6 Manuals. Available online: <https://grass.osgeo.org/grass76/manuals/r.sun.html>

HU, Y., LI, W. *DM-60 – Spatial Data Infrastructure* [online]. 2017 [cit. 2021-05-08]. UCIGIS. Available online: <https://gistbok.ucgis.org/bok-topics/spatial-data-infrastructures>

*Introduction to SLD*. 2021 [cit. 2021-05-11]. Geoserver. Available online: <https://docs.geoserver.org/stable/en/user/styling/sld/introduction.html>

INSTITUTO IDEAL AND AHK RIO. (2019). *The Brazilian Market of Distributed Photovoltaic Generation*. Rio de Janeiro, Brazil: Instituto Ideal and AHK RIO.

*Introduction to Solar Radiation* [online]. 2021 [cit. 2021-05-01]. Newport. Available online: <https://www.newport.com/t/introduction-to-solar-radiation>

*IRENA Power Generation Costs 2019*. 2021 [cit. 2021-04-03]. IRENA. Available online: [https://www.irena.org/-/media/Files/IRENA/Agency/Publication/2020/Jun/IRENA\\_Power\\_Generation\\_Costs\\_2019](https://www.irena.org/-/media/Files/IRENA/Agency/Publication/2020/Jun/IRENA_Power_Generation_Costs_2019)

*i-SCOPE Work Packages*. 2021 [cit. 2021-05-11]. i-SCOPE. Available online: <https://iscopeproject.net/project/workpackages>

KHANNA, Delphine. *Estimate solar power potential* [online]. 2021 [cit. 2021-05-11]. Available online: <https://learn.arcgis.com/en/projects/estimate-solar-power-potential/#explore-the-data>

KOLBE, Thomas. *CityGML* [online]. 2007 [cit. 2021-05-12]. Available online: <http://www.citygml.org/index.php?id=1532>

LEWIS, Colin David. (1982). *Industrial and Business Forecasting Methods*. London: Butterworth-Heinemann. ISBN 0408005599

LIANG, J., GONG, J., XIE, X., SUN, J. (2020). Solar3D: An Open-Source Tool for Estimating Solar Radiation in Urban Environments. *ISPRS International Journal of Geo-Information*, 9(9), p. 524. doi:10.3390/ijgi9090524

*Lidar 101: An Introduction to Lidar Technology, Data, and Applications* [online]. 2012-2021 [cit. 2021-04-13]. NHBC. Available online: <https://coast.noaa.gov/data/digitalcoast/pdf/lidar-101.pdf>

*Linke Turbidity (Tl) Factor Worldwide* [online]. 2021 [cit. 2021-05-01]. MINES ParisTech / Transvalor. Available online: <http://www.soda-pro.com/help/general-knowledge/linke-turbidity-factor>

LLOYD, C., ATKINSON, P. (2002). Deriving DSMs from LiDAR data with kriging. *International Journal of Remote Sensing*, 23(12). pp. 2519-2524. doi: 10.1080/01431160110097998

LOHANI, Bharat. *Principle of LiDAR* [online]. 2007-2021 [cit. 2021-03-21]. Available online: [http://home.iitk.ac.in/~blohani/LiDAR\\_Tutorial/](http://home.iitk.ac.in/~blohani/LiDAR_Tutorial/)

MAMASSIS, N., EFSTRATIADIS, A., APOSTOLIDOU, I.-G. (2012). Topography-adjusted solar radiation indices and their importance in hydrology. *Hydrological Sciences Journal*, 57(4), pp. 756-775. doi:10.1080/02626667.2012.670703

MARTIN, A. M., DOMINGUEZ, J., AMADOR, J. (2015). Applying LIDAR datasets and GIS based model to evaluate solar potential over roofs: a review. *AIMS Energy*, 3(3), pp. 326-343. doi:10.3934/energy.2015.3.326

*Modeling solar radiation*. 2021 [cit. 2021-03-21]. Esri. Available online: <https://desktop.arcgis.com/en/arcmap/10.3/tools/spatial-analyst-toolbox/modeling-solar-radiation.htm>

*Morumbi District: district of São Paulo city* [online]. 2021 [cit. 2021-04-22]. The Government of São Paulo. Available online: <http://www.prefeitura.sp.gov.br/>

MUNTEAN, M., GUIZZARDI, D., SCHAAF, E., CRIPPA, M., SOLAZZO, E., OLIVIER, J. (2018). *Fossil CO2 emissions of all world countries: 2018 Report*. Luxembourg: European Union.

*National Environmental Data Organization System - INPE*. 2019-2021 [cit. 2021-05-01]. IEA. Available online: <http://SONDA.ccst.inpe.br/>

NGUYEN, H., PEARCE, J. (2010). Estimating Potential Photovoltaic Yield with r.sun and the Open Source Geographical Resources Analysis Support System. *Solar Energy*, 84(5), pp. 831-843. doi:10.1016/j.solener.2010.02.009

NREL. (2013). *Estimating Rooftop Suitability for PV: A Review of Methods, Patents, and Validation Techniques*. Oak Ridge, TN: U.S. Department of Energy.

NYS, G.-A., POUX, F., BILLEN, R. (2020). CityJSON Building Generation from Airborne LiDAR 3D Point Clouds. *ISPRS International Journal of Geoinformation*, 9(9), p. 521. doi:10.3390/ijgi9090521

*OGC Standards: CityGML* [online]. 2021 [cit. 2021-05-13]. Open Geospatial Consortium. Available online: <https://www.ogc.org/standards/citygml>

PAGE, J., ALBUISSON, M., WALD, L. (2001). The European Solar Radiation Atlas: a valuable digital tool. *Solar Energy*, 71(1), pp. 81-83. doi:10.1016/S0038-092X(00)00157-2

*PDAL - Point Data Abstraction Library* [online]. 2021 [cit. 2021-05-13]. PDAL. Available online: <https://pdal.io/>

PDAL Documentation: *writers.gdal* [online]. 2021 [cit. 2021-05-13]. PDAL. Available online: <https://pdal.io/>

PEREIRA, E. B., MARTINS, F. R., GONÇALVES, A. R., COSTA, R. S., LIMA, F. L., RÜTHER, R., . . . SOUZA, J. (2017). *Atlas brasileiro de energia solar: 2nd edition*. São José dos Campos: INPE.

*Perspectives for the Energy Transition: Investment Needs for a Low-Carbon Energy System*. 2021 [cit. 2021-04-03]. IRENA. Available online: [www.irena.org/DocumentDownloads/Publications/Perspectives\\_for\\_the\\_Energy\\_Transition\\_2017](http://www.irena.org/DocumentDownloads/Publications/Perspectives_for_the_Energy_Transition_2017)

POLIDORI, L., HAGE, M. E. (2020). Digital Elevation Model Quality Assessment Methods: A Critical Review. *Remote Sens*, 12(32), p. 3522. doi:10.3390/rs12213522

PVWatts Calculator [online]. 2021 [cit. 2021-05-13]. NREL. Available online: <https://pvwatts.nrel.gov/>

QUASCHNING, Volker. (2016). *Understanding Renewable Energy Systems*. 2. London: Earthscan/Routledge London. ISBN 978-1844071289

RALSTON, Bruce. (2004). *GIS and public data*. 1. Clifton Park, NY: Thomson/Delmar Learning. ISBN 978-1401877811

*São Paulo: City of the World* [online]. São Paulo: São Paulo Turismo (SPTuris), 2017-2021 [cit. 2021-03-12]. Available online: [http://www.observatoriodoturismo.com.br/pdf/DADOS\\_FATOS\\_2017.pdf](http://www.observatoriodoturismo.com.br/pdf/DADOS_FATOS_2017.pdf)

SCHNEIDER, R. M., LEITE, A., MINKEL, C. "São Paulo". *Encyclopedia Britannica* [online]. 2020-2021 [cit. 2021-03-21]. Available online: <https://www.britannica.com/place/São-Paulo-Brazil>

SIANTURI, Y., MARJUKI, SARTIKA, K. (2020). Evaluation of ERA5 and MERRA2 reanalyses to estimate solar irradiance using ground observations over Indonesia region. *AIP Conference Proceeding 2223, 020002*. AIP Publishing. doi:10.1063/5.0000854

URRACA, R., HULD, T., GRACIA-AMILLO, A., MARTINEZ-DE-PISON, F. J., KASPAR, F., SANZ-GARCIA, A. (2018). Evaluation of global horizontal irradiance estimates from ERA5 and COSMO-REA6 reanalyses using ground and satellite-based data. *Solar Energy*, 164, pp. 339-354. doi:10.1016/j.solener.2018.02.059

USDA. (2008). *A Guide to LIDAR Data Acquisition and Processing for the Forests of the Pacific Northwest*. Pacific Northwest: United States Department of Agriculture.

VIGLINO, Jean Marc. *ol-ext: Extensions for OpenLayers (ol)* [online]. 2021 [cit. 2021-04-21]. Available online: <https://viglino.github.io/ol-ext/>

WALD, Lucien. (2018). *Basics in Solar Radiation At Earth Surface*. Paris: HAL Id: hal-01676634.

WANG, Shengyang. Graduate Theses and Dissertations Iowa State University: Pavement albedo assessment: methods, aspects, and implication [online]. 2015. [cit. 2021-04-21]. Available online: <https://lib.dr.iastate.edu/etd/14904/>

WANG, Zhifeng. (2019). Chapter 2 - The Solar Resource and Meteorological Parameters, In: WANG, Z. *Design of Solar Thermal Power Plants*. (2019). Cambridge: Academic Press. ISBN 978-0-12-815613-1

*What is LiDAR Data?*. 2021 [cit. 2021-04-11]. Esri. Available online: <https://desktop.arcgis.com/en/arcmap/10.3/manage-data/las-dataset/what-is-lidar-data-.htm>

WILLMOTT, C., MATSUURA, K. (2005). Advantages of the mean absolute error (MAE) over the root mean square error (RMSE) in assessing average model performance. *Climate Research*, 30, pp. 79-82. doi:10.3354/cr030079

YAMASOE, M., ROSARIO, N. É., BARROS, K. (2016). Downward solar global irradiance at the surface in São Paulo city—The climatological effects of aerosol and clouds. *Journal of Geophysical Research: Atmospheres*, 122(1). doi:10.1002/2016JD025585

ZDYB, A., GULKOWSKI, S. (2020). Performance Assessment of Four Different Photovoltaic Technologies in Poland. *Energies*, 13(1), 196. DOI:10.3390/EN13010196

ZHOU, Qiming. (2017). Digital Elevation Model and Digital Surface Model, In: V L. John Wiley & Sons (Editor), *The International Encyclopedia of Geography*. (2017). China: John Wiley & Sons, Ltd. doi:10.1002/9781118786352.wbieg0768



## **ATTACHMENTS**

# LIST OF ATTACHMENTS

## **Bound attachments:**

- Attachment 1    Irradiation data from IAG USP
- Attachment 2    Calculation output of the panel inclination adjustment

## **Free attachments**

- Attachment 3        Poster
- Attachment 4    DVD
- Attachment 5    Thesis website

## **Structure of the DVD**

Files and folders:

Raster file

    DSM\_Morumbi.tif

Realsky\_Annual solar radiation\_Morumbi.tif

Vector files

    Annual\_solar\_PV\_pot\_Morumbi.geojson

    UnsuitableBld\_Morumbi.geojson

    Buildingfootprint.geojson

    Favela\_Morumbi.geojson

    Boundary\_Morumbi.geojson

    Solar\_PV\_Morumbi.gml (CityGML)

Script

    Script for iterating the *r.sun* module from January to December

Metadata (metadata in XML format)

WEB-MAP APP (code and libraries are stored in this folder)

MastersThesis\_Rizcanofana.pdf

Link to web services.txt

**Attachment 1**

Irradiation data from IAG USP (MJ/m<sup>2</sup>)

DIA / MÊS	JAN.	FEV.	MAR.	ABR.	MAI.	JUN.	JUL.	AGO.	SET.	OUT.	NOV.	DEZ.
1	25.93	13.80	12.08	20.32	14.25	16.03	13.21	13.07	13.36	23.10	0.00	19.88
2	15.91	11.10	15.99	20.07	12.30	4.76	13.79	16.84	0.00	22.26	0.00	18.13
3	17.58	10.38	13.09	15.01	15.49	9.70	10.03	17.37	22.65	12.16	23.48	21.55
4	15.44	14.42	19.18	23.01	16.66	7.59	16.69	18.19	20.09	5.78	26.26	23.06
5	12.02	13.15	0.00	21.62	18.50	8.24	16.19	18.06	21.47	23.24	18.52	9.23
6	27.12	13.30	26.66	21.98	10.78	8.96	11.92	18.22	22.56	22.94	26.27	11.70
7	26.80	16.62	25.31	0.00	6.70	15.33	15.91	18.54	20.14	20.22	28.89	12.57
8	20.20	22.15	15.70	7.63	11.28	13.52	15.92	18.11	19.40	11.42	29.45	15.43
9	19.17	24.04	24.42	22.53	18.80	8.30	14.91	16.79	18.04	3.61	23.37	0.00
10	23.30	9.10	23.32	21.90	18.86	8.37	16.15	0.00	21.03	24.25	17.51	26.33
11	24.17	12.26	24.16	15.05	18.03	13.94	15.14	16.97	20.82	27.55	18.86	19.25
12	16.14	12.57	23.52	19.89	17.35	14.80	16.02	18.92	19.46	27.72	16.02	19.25
13	12.17	19.51	21.95	18.35	9.76	14.58	15.88	14.69	21.32	24.76	15.54	21.32
14	18.21	23.05	23.95	11.83	7.10	3.95	4.40	14.85	22.49	24.85	22.84	26.73
15	26.54	24.86	22.92	16.05	6.43	8.50	4.40	7.93	10.23	7.54	27.05	21.32
16	21.14	20.98	19.49	17.40	16.34	10.96	9.79	5.11	20.76	5.27	21.74	25.94
17	12.40	21.45	19.71	10.89	16.77	14.21	12.06	6.90	20.62	12.18	9.37	18.94
18	12.88	23.49	20.55	16.61	15.00	15.08	15.85	4.74	7.10	22.31	8.90	21.33
19	12.72	20.80	17.21	19.76	17.04	15.15	15.42	11.26	18.58	18.47	8.58	27.21
20	13.98	19.69	15.57	17.78	15.05	15.58	17.55	1.75	4.41	16.83	22.39	24.67
21	26.21	10.01	11.00	19.27	15.40	14.35	17.20	2.28	8.20	19.75	0.00	18.22
22	15.25	8.90	23.50	15.42	12.32	14.06	15.31	8.89	5.50	23.85	24.22	8.36
23	6.36	14.24	24.18	18.41	4.57	13.70	15.68	19.41	12.23	29.53	25.57	13.93
24	15.25	18.00	22.69	16.89	10.63	15.07	17.45	21.08	21.20	10.17	26.05	18.86
25	25.56	18.62	23.44	19.79	18.28	13.27	17.83	17.64	23.31	16.40	28.84	0.00
26	31.90	8.02	24.27	19.63	18.12	4.52	9.56	22.78	23.71	18.14	22.41	18.22
27	31.26	10.76	23.25	18.11	17.09	2.35	17.71	19.11	23.34	25.08	23.68	17.51
28	23.72	7.93	18.85	18.17	17.37	8.28	16.62	21.16	11.03	31.01	28.45	23.07
29	0.00	12.48	13.38	20.02	16.42	12.55	3.85	22.24	10.49	22.73	23.77	23.47
30	20.14		19.66	16.42	16.41	14.87	6.21	21.96	22.07	3.80	17.73	27.69
31	19.11		20.41		16.91		10.63	13.88		9.25		20.53
total mensal:	588.6	455.7	609.4	519.8	446.0	340.5	419.3	448.7	505.6	566.2	585.8	573.7
dias com dados:	30	29	30	29	31	30	31	30	29	31	27	29
média mensal:	19.62	15.71	20.31	17.92	14.39	11.35	13.53	14.96	17.44	18.26	21.69	19.78

**Attachment 2**

Calculation output of the panel inclination adjustment

Month	Season	Inclination	Aspect	Mean daily solar radiation (Wh/m2)
March	Autumn	Without modification	Without modification	6009.5
		Without modification	90° (head north)	6231.91
		15°	90° (head north)	6584
		<b>23°</b>	<b>90° (head north)</b>	<b>6610.26</b>
		25°	90° (head north)	6598.91
June	Winter	Without modification	Without modification	3338.52
		Without modification	90° (head north)	3634.28
		15°	90° (head north)	4329.12
		23°	90° (head north)	4595.38
		<b>25°</b>	<b>90° (head north)</b>	<b>4649.61</b>
September	Spring	Without modification	Without modification	5598.15
		Without modification	90° (head north)	5814.49
		15°	90° (head north)	6183.19
		<b>23°</b>	<b>90° (head north)</b>	<b>6235</b>
		25°	90° (head north)	6231.74
December	Summer	Without modification	Without modification	7884.34
		<b>no optimization</b>	<b>90° (head north)</b>	<b>7952.86</b>
		15°	90° (head north)	7293.44
		23°	90° (head north)	6798.98
		25°	90° (head north)	6657.89